NOVA SCHOOL OF SCIENCE & TECHNOLOGY

DEPARTMENT OF
MECHANICAL AND INDUSTRIAL ENGINEERING

EDGAR ISAÍAS BELO
BSc in Mechanical Engineering Sciences

A COMPREHENSIVE METHODOLOGY FOR DEVELOPING SPECIFIC CUTTING ENERGY MODELS - APPLICATION IN END MILLING OF 1.2738 HH TOOL STEEL

MASTER IN MECHANICAL ENGINEERING
NOVA University Lisbon
september, 2022

NOVA SCHOOL OF SCIENCE & TECHNOLOGY

DEPARTMENT OF
MECHANICAL AND INDUSTRIAL ENGINEERING

A COMPREHENSIVE METHODOLOGY FOR DEVELOPING SPECIFIC CUTTING ENERGY MODELS – APPLICATION IN END MILLING OF 1.2738 HH TOOL STEEL

EDGAR ISAÍAS BELO

BSc in Mechanical Engineering Sciences

Adviser: Carla Maria Moreira Machado
Assistant Professor, NOVA University Lisbon

Co-advisers: António José Freire Mourão
Associate Professor, NOVA University Lisbon

Examination Committee:

Chair: Telmo Jorge Gomes dos Santos,
Full Professor, NOVA University Lisbon

Rapporteurs: Pedro Alexandre Rodrigues Carvalho Rosa,
Associate Professor, *Instituto Superior Técnico*

Adviser: Carla Maria Moreira Machado,
Assistant Professor, NOVA University Lisbon

MASTER IN MECHANICAL ENGINEERING

NOVA University Lisbon
september, 2022

A Comprehensive Methodology for Developing Specific Cutting Energy Models – Application in End Milling of 1.2738 HH Tool Steel

To my parents,

for their efforts, dedication and love.

ACKNOWLEDGMENTS

It was five tough years. This work is the result of commitment, dedication and effort. However, it was not possible to do it without some people that really supported me along this journey.

First, I want to express all my gratitude to my adviser, Professor Carla Machado, and my co-adviser, Professor António Mourão, for their guidance during the development of this dissertation. The support provided by both Professors was tireless, always revealing their greatest interest and enthusiasm to help me every time I needed. Additionally, I am deeply grateful for the values that were transmitted to me, which I am sure will be an asset in my personal life and my future professional career.

Next, I want to leave my sincere gratitude to Pedro Fonseca, Pedro Rendas, Francisco Ribeiro, Mr. Wagner Sabor, Mr. António Campos and Mr. Paulo Magalhães, for their friendship, advice and constant readiness to help me in the lab.

To my course friends, partners during these five long years, Diogo Matos and Rafaela Correia, for their friendship, support, camaraderie and shared effort. The motto was always clear: nobody is left behind.

Now, I want to leave my deepest appreciation to my father, Miguel, and my mother, Patrícia, for giving me all I need, when I need. For the support during the course, for make me feel that, even in the most difficult times, there is always a safe place called Home, waiting for us any time, where we can rest and recover for the remaining duties. To my brother Salvador, for his pure admiration for me. His happiness when I was returning home was something special and filled me with pride. I know I am an example for him and may my path be a reference for his future.

To my grandparents, José, Maria dos Santos and Maria da Conceição, for all the affection, care and attention given.

I extend my acknowledgements to my godmother, Ângela, my uncle António, and my cousins Tomás and Maria Inês, for receiving me in their home in Lisbon, particularly during all the first year of the course. In a such difficult year, I was treated like a son, and I will never be able to express my complete gratitude. In the same way, I would like to thank my aunt, Cândida, my godfather, Ricardo, my cousin, Daniel, Constança and Marlene, for welcoming me in their homes when I needed, for supporting me during the weeks that I spent in Lisbon. Many times, their homes were a shelter to me, to get away from the intensity of the week. I was very lucky to have family close to me during these years.

For last, but not the least, I want to express my gratitude to my best friend, my partner in the most difficult hours, my girlfriend, Maria, for her attention, patience, and love. For hearing me, late at night, about my problems, my fears, my apprehensions, and for motivating me, day after day, to follow my path.

To all of you, my deepest recognition and respect.

“Somewhere, something incredible is waiting to be known.” (Carl Sagan).

ABSTRACT

The continuous growth and expansion of manufacturing industry brings the need to focus on sustainable manufacturing, in order to reduce both economic and environmental impacts. The specific cutting energy is a quantity that reflects the energy required to remove a unit volume of material and a good indicator of the efficiency of a machining process. Several empirical models that allow to estimate this indicator as function of the cutting parameters, which are a powerful tool to assist in process planning, can be found in literature. However, the use of the same known models for any type of cutting processes, materials and cutting tools can lead to less accurate estimates of specific cutting energy, thus preventing the achievement of a more efficient machining process. Thus, the aim of this dissertation is to develop a suitable methodological process from which a practical model to estimate specific cutting energy can be established, for application during end milling of 1.2738 HH tool steel, using S710 end mill from Dormer. For that purpose, Design of Experiments (DoE), Analysis of Variance (ANOVA) and Response Surface Methodology (RSM) were firstly applied to determine the influence of the machining parameters (feed per tooth, cutting speed and depth of cut) on specific cutting energy, to quantify the correlation between the parameters and this indicator and, ultimately, to gain a better understanding about the overall process behaviour, by means of a polynomial model. Afterwards, the results from these statistical approaches enabled to formulate a simple and practical model of specific cutting energy as function of only the most influent cutting parameters identified previously. Finally, the model was subjected to a validation procedure. The acquired results revealed that the model provided accurate estimates of specific cutting energy. Furthermore, in comparison with other empirical models, lower estimates were obtained.

Keywords: 1.2738 HH Tool Steel, Analysis of Variance, End Milling, Response Surface Methodology, Specific Cutting Energy

Resumo

O crescimento e expansão da indústria transformadora contribui para o surgimento de uma ideologia focada na produção sustentável, de forma a reduzir os seus impactos económicos e ambientais. A energia específica de corte é uma grandeza que reflete a energia necessária à remoção de uma unidade de volume de material e um bom indicador da eficiência de um processo de maquinagem. Diversos modelos empíricos que permitem estimar este indicador em função dos parâmetros de corte podem ser encontrados na literatura, os quais são uma ferramenta de auxílio à preparação de trabalho. Contudo, o uso dos mesmos modelos para qualquer tipo de processos de corte, materiais e ferramentas pode conduzir a estimativas menos precisas da energia específica de corte, o que consequentemente impede o alcance de uma maior eficiência ao longo de um determinado processo. Assim, o objetivo desta dissertação é desenvolver uma metodologia a partir da qual um modelo para estimar a energia específica de corte possa ser estabelecido, para aplicação durante a fresagem de topo do aço 1.2738 HH, utilizando uma fresa de topo S710 da Dormer. Para tal, o Desenho de Experiências (DE), Análise de Variância (AV) e a Metodologia da Superfície de Resposta (MSR) foram utilizados para determinar a influência dos parâmetros de maquinagem (avanço por dente, velocidade de corte e profundidade de corte) na energia específica de corte, quantificar a correlação entre os parâmetros e este indicator e, em ultima instância, para melhor compreensão do comportamento global do sistema, por meio de um modelo polinomial. Posteriormente, os resultados provenientes destas abordagens estatísticas permitiram formular um modelo de energia específica de corte em função apenas dos parâmetros de corte mais influentes. Por fim, o modelo foi submetido a um procedimento de validação. Os resultados obtidos revelaram que o modelo forneceu estimativas precisas de energia específica de corte. Em comparação com outros modelos empíricos, foram obtidas estimativas inferiores deste indicador.

Palavras chave: Aço 1.2738 HH, Análise de Variância, Energia Específica de Corte, Fresagem de Topo, Metodologia da Superfície de Resposta

CONTENTS

LIST OF FIGURES

LIST OF TABLES

ACRONYMS

ANOVA	Analysis of Variance
ASME	*American Society of Mechanical Engineers*
AWF	*Ausschuss für Wirtschaftliche Fertigung*
CCD	Central Composite Design
DoE	Design of Experiments
DOF	Degrees of Freedom
HSM	High Speed Machining
MS	Mean Square
RSM	Response Surface Methodology
SS	Sum of Squares
USEIA	United States Energy Information Administration

SYMBOLS

A_c	Cutting Area [mm^2]
b	Cutting Width [mm]
C_a	ASME Constant of the Material to be Machined
C_w	AWF Constant of the Material to be Machined
D	Diameter of the Cutting Tool [mm]
f	Feed Rate [mm/rev]
F	Feed Speed [mm/min]
F_{ac}	Active Force [N]
F_c	Cutting Force [N]
F_f	Feed Force [N]
F_p	Passive Force [N]
F_R	Resultant Force [N]
F_s	Support Force [N]
f_z	Feed per Tooth [mm/tooth]
h	Cutting Thickness [mm]
h_m	Average Chip Thickness [mm]
K_c	Specific Cutting Force [N/mm^2]
K_{c1}	Specific Cutting Force to Cut a Chip Area of 1 mm^2 with a Thickness of 1 mm [N/mm^2]

K_s	Specific Cutting Energy [J/mm^3]
N_c	Cutting Power [W]
p	Depth of Cut [mm]
S	Spindle Speed [min^{-1}]
t	Radial Depth of Cut [mm]
v_c	Cutting Speed [m/min]
z	Correcting Factor for the Average Chip Thickness
Z	Number of Cutting Edges
Z_M	Material Removal Rate [mm^3/s]
φ	Angle of Feed Direction

1

INTRODUCTION

1.1 Motivation and Objectives

The Annual Energy Review book [1], published by the United States Energy Information Administration (USEIA) in 2012, revealed that 31% of the total electricity consumption of the end-use sector is related to the industrial sector. Manufacturing is an important part of the industrial sector, playing an important role in the global economy [2]. The manufacturing principle is to convert raw materials into products and, as it consumes a large amount of resources, environmental wastes and emissions are a concern about this sector [3, 4]. To support the continuous growth and expansion of manufacturing industry, sustainable manufacturing has been a focus in recent years [3], which was triggered by increasing energy costs, political and environmental demands [5]. Expectedly, scientific studies directed towards energy consumption and its subsequent preservation are constantly increasing, in order to reduce both economic and environmental impacts.

Machining is one of the major activities in manufacturing industries, being responsible for a significant part of the total energy consumed by this sector [6]. The total energy consumption in machining derives from the product between the specific cutting energy and the total volume of material removed [7]. Several empirical models to estimate specific cutting energy as function of the cutting parameters, namely feed per tooth and depth of cut, can be found in literature. These simple and practical models prove to be a powerful tool to assist in process planning, allowing not only to determine the set of cutting parameters that lead to a lower specific cutting energy, but also to estimate the cutting forces inherent to the machining

process, thus contributing to achieve a more efficient process through a proper selection of cutting parameters, machine tools and cutting tools.

It turns out that the use of these models is not restricted to one particular type of cutting process, workpiece material and cutting tool, all of these factors that affect the specific cutting energy. However, for example, situations exist where the models do not take in consideration the effect of a certain cutting parameter, which in fact is significant for the specific cutting energy for the particular combination cutting operation / workpiece material / cutting tool selected. Thus, the model will not reflect this indicator accurately, which prevents to achieve a more efficient process. The motivation of this dissertation arises from the need to conduct studies aimed at formulating not one, but several simple and practical models to estimate specific cutting energy, restricted for a particular machining process, material and cutting tool, with the purpose of improving its estimates.

Therefore, the objective of this work is to develop a proper methodology that provides a comprehensive guidance to formulate a practical model of specific cutting energy for application during end milling of 1.2738 HH tool steel.

1.2 Structure of the Dissertation

The present dissertation is structured in six chapters: Introduction, Literature Review, Methodology, Experimental Procedure, Experimental Results and Discussion and finally Conclusions and Future Work. A brief description of each of the chapters is presented next.

Chapter 1 – Introduction – presents the main motivations and objectives established for this dissertation.

Chapter 2 – Literature Review – is related to the review of the literature concerning some scientific investigations made in the recent years related to the specific cutting energy and the theoretical concepts related to the milling processes, for a better understanding of the subject.

Chapter 3 – Methodology – addresses the methodology applied in this work, described by several detailed flowcharts, thus providing a comprehensive step by step guidance for conducting studies in the same research line. DoE, ANOVA and RSM are analysed to

understand the theory behind these used techniques, the purpose of its application in this dissertation and how they should be applied in order to acquire appropriate data.

In Chapter 4 – Experimental Procedure – an exhaustive description of the experimental work is done. In this chapter, the material and cutting tool are characterized and all the equipment used to perform the experiments is fully detailed for a better understanding about how the data is acquired and treated in order to achieve the proposed objectives.

In Chapter 5 – Experimental Results and Discussion – the acquired results are discussed and the main findings are presented. The evolution of the cutting forces during an experimental trial and the results of ANOVA and RSM are presented, the process underlying the formulation of the specific cutting energy model is addressed and finally the model is validated through a series of validation tests. Further, the estimates provided by other empirical models are compared to the results of the validation tests.

Chapter 6 – Conclusions and Future Work – presents the conclusions of the dissertation and further recommendations and suggestions for future work related to this subject.

2

LITERATURE REVIEW

2.1 State of the Art

In recent years, due to the modern concern of sustainability, a lot of machining research for several types of machining processes and different nature materials was carried out regarding the specific cutting energy. A large part of these studies is related to the analysis and optimization of the cutting process through statistical approaches. Notably, the statistical optimisation methods have proven to be very powerful and reliable tools [8].

Camposeco-Negrete [9] optimised the cutting parameters for minimizing specific cutting energy in roughing turning of AISI 6061 T6 aluminium under conventional flood lubrication, using RSM. A regression model giving the correlation between the cutting parameters and specific cutting energy was obtained, whose adequacy was proved by the ANOVA technique. It was noticed that the most influent factors were depth of cut and feed rate, with depth of cut being more preponderant. Both factors contributed to a minimization of specific cutting energy when they were at their maximum level. Campatelli et al. [10] conducted a study focused on the efficiency of the cutting process, which is mainly related to the specific cutting energy. Using RSM, the authors evaluated the influence of the process parameters (cutting speed, feed rate, axial and radial depths of cut) on specific cutting energy by obtaining a model fit for the fine tuning of the process parameters during milling of AISI 1050 carbon steel. The most influent parameters were feed per tooth and radial depth of cut. Jaffery et al. [11] carried out a study in which specific cutting energy was analysed in relation to the process parameters, during turning Ti-6Al-4V titanium alloys under dry condition. Applying Taguchi Design of Experiments method and ANOVA technique, the authors found that feed rate was the most

significant parameter, followed by the cutting speed. A decreasing trend of specific cutting energy was observed with an increase in both feed rate and depth of cut. Lima et al. [12], keeping the cutting speed constant, studied the influence of feed per tooth and depth of cut on specific cutting energy during face milling of 6351-T6 aluminium alloy, using a Two Factor Factorial Design. The ANOVA results showed that feed per tooth was observed to be the parameter with the major effect.

Following this topic, other authors extended their research to understand the impact that other factors may have on specific cutting energy. Wang et al. [13] revealed the influence of cutting speed, undeformed chip thickness and tool rake angle on this indicator during high-speed machining (HSM) of 7050-T7451 aluminium alloy. They pointed that tool rake angle had an important effect, being its influence more evident with the increase of cutting speed. Mozammel Mia [14] developed a work with several purposes during end milling of AISI 4140 steel. The author aimed to quantify the effects of cutting speed, feed rate and flow rate of lubricant on specific cutting energy, to develop a mathematical model of this indicator using RSM and to optimise the process parameters along with the determination of optimum parameter setting using Taguchi method.

The aforementioned literature survey demonstrates that, through statistical analysis, efforts have been made towards optimisation of cutting parameters with the purpose of minimizing the specific cutting energy and determination of the effect that the cutting parameters and other factors, such as the geometric characteristics of the cutting tool, may have on this indicator, for different machining processes and materials. Moreover, using these statistical approaches, it was pointed that some researchers have also focused on presenting mathematical models of specific cutting energy. Such polynomial models are an appropriate tool to quantify the correlation between the cutting parameters and the desired response and to study the global behaviour of the system within a certain experimental range. However, regarding its application in process planning, these models are not appropriate to calculate specific cutting energy in a simple and practical way, which comprises its value in this subject.

Nevertheless, no work has been conducted to follow up on the results obtained from these statistical studies in order to obtain a simple and practical model to estimate specific cutting energy. Therefore, the aim of this dissertation is to develop a methodology that allows to formulate a model to predict this quantity, involving firstly a statistical analysis performed

using DoE, ANOVA and RSM. Afterwards, the model intended to be formulated will be developed based on the results obtained through these statistical approaches.

2.2 Milling

A cutting operation is defined as an operation that, by giving the component its shape, dimensions, finishing, or a combination of the previous factors, produces chip. The chip is the portion of the material removed from the workpiece, characterized by an irregular morphology [15].

Milling is a mechanical process in which a rotary cutting tool, with multiple cutting edges, is responsible for material removing by advancing into the workpiece material. Typically, the cutting tool is fixed in the machine holder and the work table provides the feed movement. Through this cutting process, a large number of different surfaces can be obtained, depending on the relative movement between the workpiece and the cutting tool [16]. In addition to all the conventional applications, milling is a strong alternative for producing holes, threads, cavities and surfaces that used to be turned, drilled or taped [17].

Two basic types of milling operations can be distinguished, namely tangential milling (Figure 2.1) and frontal milling (Figure 2.2) [15]. The former is characterized by obtaining a planar surface parallel to the rotational axis of the cutting tool, whereas the latter consists in machine a surface that is perpendicular to the axis of the cutter. When the machined surface is a non-planar surface (Figures 2.3a and 2.3c) or the rotational axis of the cutting tool is not parallel to the obtained surface (Figure 2.3b), the machining process is a special variant of tangential milling [15]. In the same way, there are some special variants of frontal milling (Figure 2.4). Moreover, there are some cases that both types of milling presented above can be present simultaneously (Figure 2.5). There may be, or not, a predominance of one type over the other.

In a milling operation, the workpiece is fed either with or against the direction of the cutter rotation, which affects the start and the finish of the cut if climb milling (down milling) or conventional milling (up milling) method is used. In conventional milling (Figure 2.1a), the feed direction is opposite to the rotation of the cutter. The chip thickness is initially equal to zero and starts to increase from the beginning of the cut. The cutter tends to lift the workpiece

from the table, increasing the clearances between the table and bed or saddle ways, which lead to vibrations that impair the surface finish produced on the work when making heavy cuts [18]. In down milling (Figure 2.1b), the workpiece is fed with the rotation direction so that the workpiece is pushed into the fixture or towards the table [18], holding the cutting edge in the cut. The chip thickness starts to decrease from the beginning of the cut until it reaches zero at the end of the cut. Therefore, the cutting tool is subjected to maximum load from the very beginning [18]. If the part has a foundry skin or is covered with scale, cutter life is substantially reduced because the teeth must cut through the very hard and abrasive surface [18]. Thus, this type of milling is preferred when machining parts with sandy or scaly surfaces because their detrimental effect on cutter life is less pronounced [18].

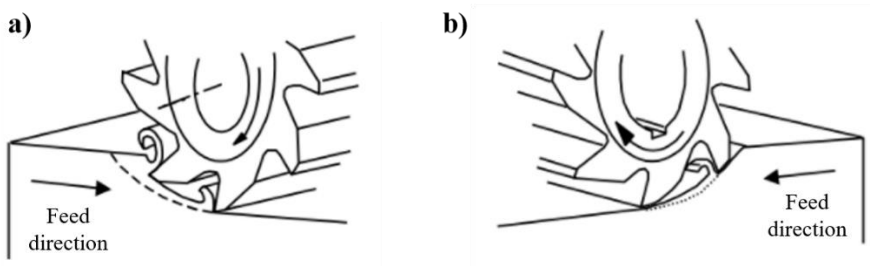

Figure 2.1 Tangential milling: a) Up milling; b) Down milling [15]

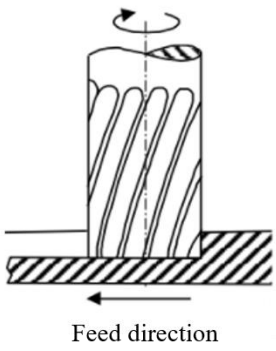

Figure 2.2 Frontal milling [15]

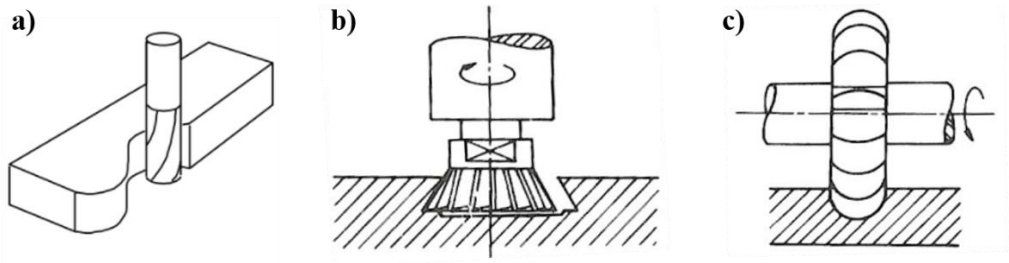

Figure 2.3 Special variants of tangential milling: a) Contour milling; b) Swallow tail slot milling; c) Profile milling [15]

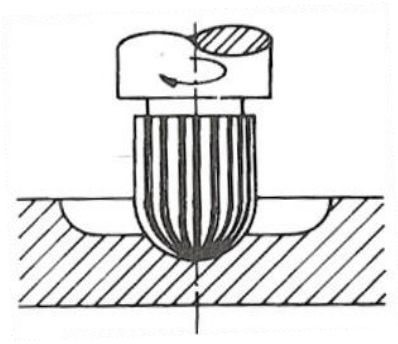

Figure 2.4 Special variant of frontal milling [15]

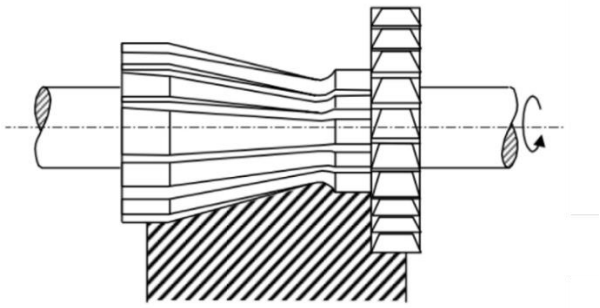

Figure 2.5 Composed milling [15]

2.2.1 Movements and directions

During a machining process, there are relative movements between the cutting tool and the workpiece [15]. Two different types of movements are distinguished: those that interfere with the chip removal process and those that do not [15]. In the next sub-chapters, the movements that originate the chip removal during the milling process, thus generating the final machined surface, will be analysed. The movements are described in relation to the part, considered as fixed.

2.2.1.1 Cutting movement

The cutting movement is the motion between the part and the tool that, without the feed movement, would originate only a single chip removal, during a revolution of the cutting tool [15] (Figure 2.6). The instantaneous direction of the cutting movement is called cutting direction [15].

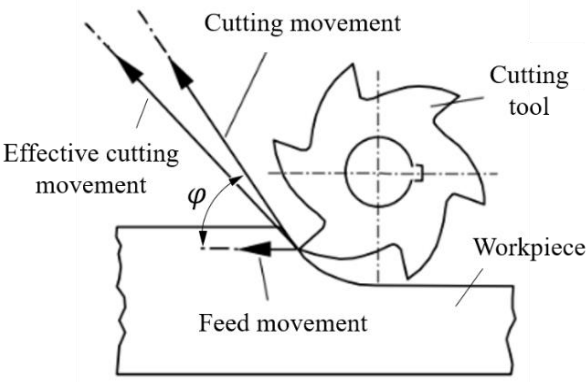

Figure 2.6 Movements between the cutting tool and the workpiece [15]

2.2.1.2 Feed movement

The feed movement is the motion between the workpiece and the cutting tool that, when combined with the cutting movement, leads to a continuous chip removal during multiple revolutions of the cutting tool [15] (Figure 2.6). The feed direction is the instantaneous direction of the feed movement.

The instantaneous angle φ between the cutting direction and the feed direction is the angle of feed direction [15]. Figure 2.7 (adapted from [15]) depicts the variation of the angle φ during a slot milling operation.

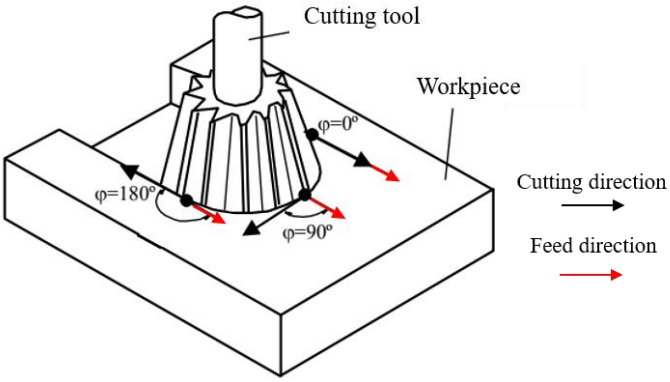

Figure 2.7 Variation of the angle φ during slot milling

2.2.1.3 Effective cutting movement

The effective cutting movement is the resultant motion of both cutting and feed movements [15] (Figure 2.6). The instantaneous direction of the effective cutting movement is nominated effective cutting direction [15].

2.2.2 Cutting parameters

The cutting parameters are the physical quantities inherent to the cutting process that affect the machining performance. These parameters must be adjusted and applied to the machine tool in order to unleash the cutting process [16]. The cutting parameters are the following:

- Cutting speed;
- Feed rate;
- Axial depth of cut;
- Radial depth of cut.

The formulas used to predict these cutting parameters, which will be used along this dissertation, will be presented further in the next sub-chapters.

2.2.2.1 Cutting speed

The cutting speed, v_c [m/min], is the instantaneous speed of the cutting edge, according to the cutting direction [15]. The cutting speed is given by Equation (2.1) [18], in which D [mm] is the diameter of the cutting tool and S [min^{-1}] is the spindle speed of the machine tool.

$$v_c = \frac{\pi \cdot D \cdot S}{1000} \quad \textbf{(2.1)}$$

Tool manufacturers provide in their catalogues recommendations about the cutting speed that should be used according to the cutting tool chosen to perform the operation and the material to be machined. In this study, the cutting speed was adjusted within the tool manufacturers' recommendations. Thus, the spindle speed of the machine tool can be predicted through Equation (2.1) as well. The limit of the spindle speed of the machine tool must be regarded.

2.2.2.2 Feed rate

Feed rate, f [mm/rev], is defined as the progression of the cutting tool during a revolution [15]. In cutting tools with several cutting edges, another parameter must be considered. Similarly to feed rate, the feed per tooth, f_z [mm/tooth], is the progression of each cutting edge during a rotation of the cutter, measured in the feed direction [15]. Equation (2.2) [15] allows to calculate feed rate, as function of feed per tooth and the number of cutting edges, Z.

$$f = f_z \cdot Z \quad \textbf{(2.2)}$$

As seen before, there is a straight relationship between the cutting speed and the spindle speed. Likewise, feed rate determines the feed speed, F [mm/min], which is the parameter considered by the machine tool to perform the cutting operation. Given by Equation (2.3) [18], it is the instantaneous speed of the cutting tool, according to the feed direction [15].

$$F = f \cdot S \quad \textbf{(2.3)}$$

2.2.2.3 Axial depth of cut

The axial depth of cut, p [mm], is the length of the cutting edge that actually intervene in the cutting process, measured in a direction normal to the work plane (Figure 2.8) [16]. Along this work, the axial depth of cut is referred to as just depth of cut.

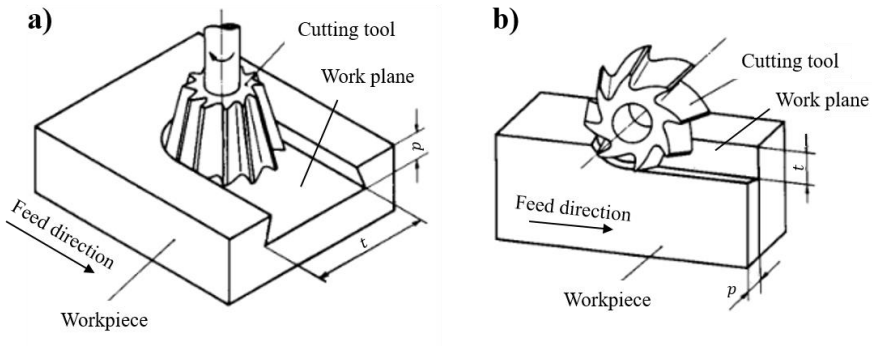

Figure 2.8 Axial and radial depths of cut in: a) Frontal milling; b) Tangential milling [15]

2.2.2.4 Radial depth of cut

The radial depth of cut, t [mm], is the dimension of the machined zone measured in the work plane, normal to the feed direction (Figure 2.8) [15]. It should be noted that the axial and radial depths of cut are two quantities measured perpendicularly to each other [16].

2.2.3 Chip-related quantities

The quantities related to the chip removed during the cutting process, namely cutting width and cutting thickness, derive from the cutting parameters used to perform the operation [15]. The following sub-chapters present the formulas used in the present dissertation to predict these quantities.

2.2.3.1 Cutting width

The cutting width (or width of cut), b [mm], is the width of the chip removed during the cutting operation (Figure 2.9). This dimension is measured along the cutting edge and equals the length of contact between the cutter tooth and the part [18].

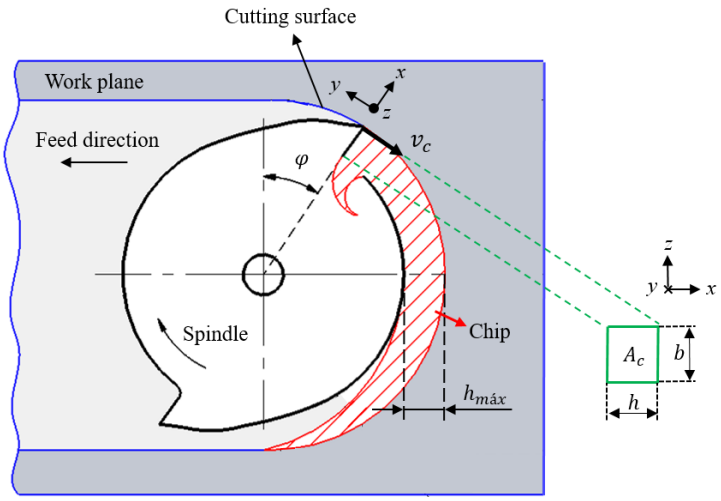

Figure 2.9 Chip formation mechanism for a straight-flute cutter in slot milling

For a straight-flute cutter, the correlation presented by Equation (2.4) [18] is established. In case of a helical-flute cutting tool, the cutting width is not constant and varies during the cutting process. Thus, its determination is not obvious. In this research work, a cutting tool with a certain helix angle was used, as will be presented in chapter 4.2.3. However, due to the low values of depth of cut established for this study, the correlation given by Equation (2.4) will be considered as an approximation to calculate the value of the cutting width.

$$b = p \tag{2.4}$$

2.2.3.2 Cutting thickness

The cutting thickness (or chip thickness), h [mm], is the thickness of the chip derived from the cut. It corresponds to the variable distance between consecutive cut surfaces. This quantity, usually referred as undeformed chip thickness, is measured in a direction normal to the initial cut surface at the point being considered, i.e. the chip thickness is measured in the radial direction and varies along the whole arc of contact between the cutter and the part [18] (Figure 2.9).

In case of a straight-flute cutter, the cutting edge enters the cut and exists simultaneously along the whole width of cut. Thus, the cutting thickness is constant along the length of the cutting tooth and can be determined through Equation (2.5) [18]. In this expression, as referred

before, φ is the angle of feed direction, which also corresponds to the instantaneous tooth contact angle. In slot milling, the chip thickness reaches its maximum value when $\varphi = 90^{o}$. Thus, at this point, the correlation given by Equation (2.6) is verified.

$$h = f_z \cdot \sin \varphi \quad \textbf{(2.5)}$$

$$h_{max} = f_z \quad \textbf{(2.6)}$$

For a helical-flute cutting tool, the tooth enters and leaves gradually the cut, which leads to a variable chip thickness, both along the length of the full arc of contact and the length of the active portion of the tooth [18]. For this type of cutters, the chip thickness is calculated by Equation (2.5) as well. However, there will exist two different instantaneous tooth contact angles, depending on the initial and final positions of the active portion of the tooth. Likewise, the maximum value of the cutting thickness is obtained by Equation (2.6). As done previously in case of width of cut, an approximation will be made and the analysis will be carried out considering that the chip thickness is constant along the whole width of cut and only varies along the length of the full arc of contact between the tool and the part.

2.2.3.3 Cutting area

The cutting area, A_c [mm^2], is the cross section of the chip removed and it is measured in the plane normal to the cutting direction [15] (Figure 2.9). Equation (2.7) allows to predict the cutting area, by multiplying the cutting width by the cutting thickness.

$$A_c = b \cdot h \quad \textbf{(2.7)}$$

As stated before, the cutting width is constant and equal to the depth of cut. Thus, the cutting area is maximum when the cutting thickness reaches its maximum value. As pointed before in chapter 2.2.3.2, at this point the cutting thickness corresponds to feed per tooth. Thus, the maximum cutting area can be obtained through Equation (2.8).

$$A_{c_{max}} = p \cdot f_z \quad \textbf{(2.8)}$$

2.2.4 Cutting forces

The cutting forces are an important indicator for evaluating a machining process [19]. The knowledge of the cutting forces is the basis for a better understanding of the metal cutting process behaviour, leading to an efficient process through the proper selection of cutting parameters, machine tools, fixtures and cutting tools [20]. As stated by Hoang et al. [19], a reliable quantitative prediction of cutting forces is critical to predict the power requirements of the machine tools. Factors such as the material to be machined, cutting parameters, material of the cutting tool and its geometrical characteristics, affect the cutting forces [21]. In this dissertation, the monitoring of the cutting forces will allow to calculate specific cutting energy for each experiment.

Figure 2.10 depicts the cutting forces during a milling operation. The resultant force that acts at the tip of the cutting edge, F_R [N], can be decomposed in two components, namely the active force, F_{ac} [N], located in the work plane, and the passive force, F_p [N], normal to the work plane. Due to its perpendicularity to the work plane, the passive force only contributes for a small portion of the total resultant force. Thus, its contribution for the machining power is reduced when compared to the contribution of the active force. The correlation between the last three forces is expressed by Equation (2.9) [21].

$$F_R = \sqrt{{F_{ac}}^2 + {F_p}^2} \tag{2.9}$$

In addition, the active force can be decomposed in two components. Its projection in the feed direction is called the feed force, F_f [N], whereas the support force, F_s [N], is the projection of the active force in a direction normal to the feed direction, located in the work plane. The active force can be obtained through Equation (2.10) [15].

$$F_{ac} = \sqrt{{F_f}^2 + {F_s}^2} \tag{2.10}$$

The cutting force, F_c [N], usually named as the main cutting force, is the projection of the resultant force in the cutting direction (given by the cutting speed). When the angle φ

between the cutting direction and feed direction is equal to 90º (Figure 2.11), the support force coincides with the cutting force. In this case, the active force is defined by Equation (2.11) [15].

$$F_{ac} = \sqrt{{F_c}^2 + {F_f}^2} \quad \textbf{(2.11)}$$

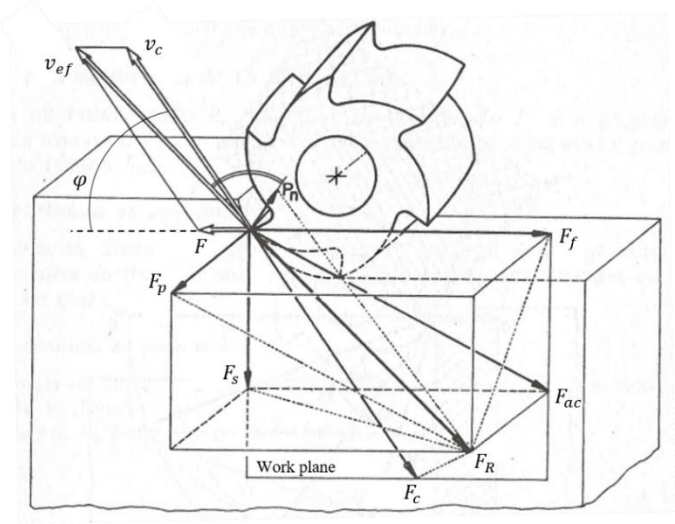

Figure 2.10 Forces in milling process [15]

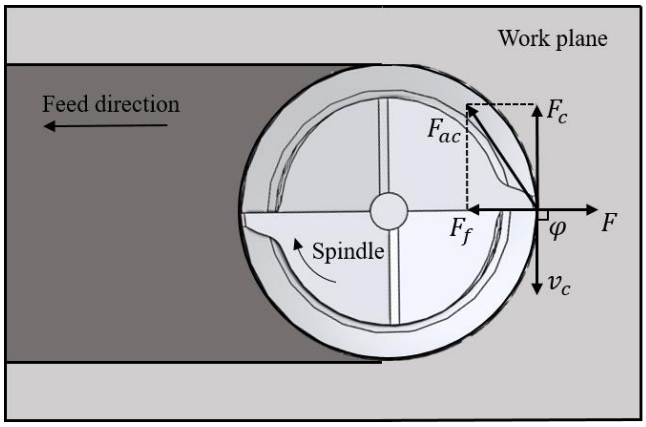

Figure 2.11 Forces at the tip of the cutting edge when φ = 90º

2.2.5 Specific cutting energy

The specific cutting energy is defined as the amount of energy required to remove a unit volume of work material and can be used as an efficiency indicator of the machining process [22]. It is dependent upon the machinability of the material and the cutting conditions,

so it can be easily controlled by the operators [23]. Additionally, other factors such as the cutting tool or the cutting process to be performed affect the specific cutting energy [24].

2.2.5.1 General model

In general, the specific cutting energy, K_s [J/mm^3] is obtained by Equation (2.12), dividing the cutting power, N_c [W], by the material removal rate, Z_M [mm^3/s].

$$K_s = \frac{N_c}{Z_M} \tag{2.12}$$

The cutting power results from the product between the cutting force and the cutting speed, whereas the material removal rate is obtained by multiplying the cutting area by the cutting speed. Considering this, Equation (2.12) can be rewritten, being the specific cutting energy, now expressed in [N/mm^2], obtained by the quotient between the cutting force and the cutting area, as presented by Equation (2.13). Dimensionally, the specific cutting energy is a pressure. Regarding this, it can be named as specific cutting pressure [16] or, according to several tool manufacturers such as Dormer and Sandvik Coromant, as specific cutting force [17, 25]. It should be noted that both measurement units of specific cutting energy expressed before are valid. However, in this dissertation, specific cutting energy will be expressed always in [J/mm^3].

$$K_s = \frac{F_c}{A_c} \tag{2.13}$$

Figure 2.9, presented in sub-chapter 2.2.3.1, shows that the cutting thickness is not constant, which causes the cutting area to vary periodically with the rotation of the cutting tool. It was already pointed that the maximum value of the cutting area is calculated by multiplying depth of cut by feed per tooth. Moreover, the higher the value of the cutting area, the higher the value of the cutting force needed to cut the material. Therefore, the specific cutting energy can be calculated by the quotient between the maximum cutting force and the maximum cutting area, through Equation (2.14).

$$K_s = \frac{F_{c_{max}}}{p \cdot f_z} \quad \textbf{(2.14)}$$

2.2.5.2 Other empirical models

There are several models in literature that allow the calculation of specific cutting energy. These objective expressions are very useful in terms of process planning, because they allow an immediate estimation of this quantity as function of the cutting parameters. Taylor studied the dependence of specific cutting energy with the cutting section and proposed three different expressions depending on the material to be machined. Equations (2.15) - (2.17) [15] allow to estimate this indicator during machining of grey cast iron, white cast iron and mild carbon steel, respectively. The meaning of each variable was already presented. In these models in particular, the specific cutting energy is given in [daN/mm^2].

$$K_s = \frac{88}{{f_z}^{0.25} \cdot p^{0.07}} \quad \textbf{(2.15)}$$

$$K_s = \frac{138}{{f_z}^{0.25} \cdot p^{0.07}} \quad \textbf{(2.16)}$$

$$K_s = \frac{200}{{f_z}^{0.2}} \quad \textbf{(2.17)}$$

Additionally, organizations such as *American Society of Mechanical Engineers* (ASME) and *Ausschuss für Wirtschaftliche Fertigung* (AWF) developed models to predict specific cutting energy, similar to those proposed by Taylor. Equation (2.18) [15] shows the model proposed by ASME, where C_a is a constant of the material to be machined, and n is dependent on the material as well: 0.2 for steels and 0.3 for cast iron. Equation (2.19) [15] presents the correlation established by AWF, in which C_w represents a material constant. In both Equations (2.18) and (2.19), the specific cutting energy is given in [daN/mm^2], as in the models proposed by Taylor.

$$K_s = \frac{C_a}{f_z^{\,n}} \tag{2.18}$$

$$K_s = \frac{C_w}{f_z^{\,0.477}} \tag{2.19}$$

The values of C_a and C_w are tabulated for different types of materials. However, both constants are defined for some specific characteristics of the cutting tool, which are presented in Table 2.1. In case of C_a, the values are valid when using a high-speed steel cutting tool (18% W, 4% Cr, 1% V). For C_w, AWF does not specify the type of material of the cutting tool. Figure 2.12 depicts a comparative analysis between the values of specific cutting energy predicted according to the aforementioned models.

Table 2.1 Geometrical characteristics of the cutting tools used by ASME and AWF [15]

	C_a	C_w
Position angle	60º	40º
Back rake	8º	-
Relief	6º	-
Side rake	14º	-
End cutting edge angle	6º	-
Side cutting edge angle	30º	-
Nose radius	1/4''	-

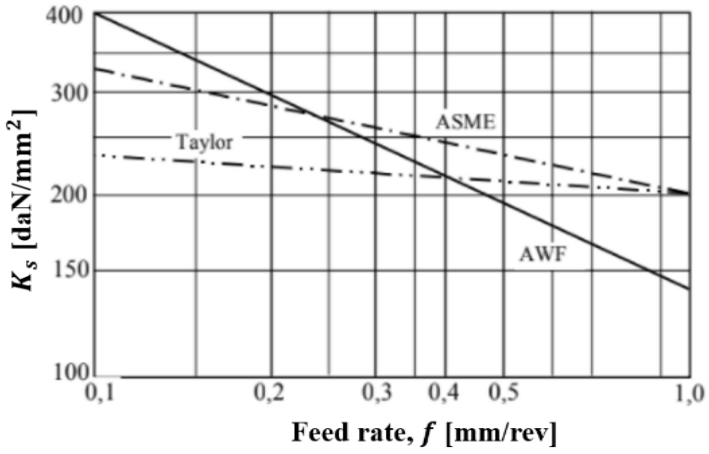

Figure 2.12 Comparative analysis between the models proposed by Taylor, ASME and AWF [15]

Some other models to estimate specific cutting energy are proposed by tool manufacturers. Dormer presented a formula to predict this indicator specified for milling processes (Dormer refers to specific cutting energy as specific cutting force, K_c), given by Equation (2.20) [25], in which K_{c1} [N/mm^2] is the specific cutting force needed to cut a chip area of 1 mm^2 that as a thickness of 1 mm, h_m [mm] is the average chip thickness (as showed before, this can be considered the feed per tooth), and z is a correcting factor for the average chip thickness. In this case, the specific cutting force is given in [N/mm^2].

$$K_c = K_{c1} \cdot {h_m}^{-z} \tag{2.20}$$

2.2.5.3 Final remarks

It is noted that all the previous models establish a correlation between specific cutting energy and the cutting parameters. The general model, given by Equation (2.13), is obtained by dividing the cutting force by the cutting area. In this expression, the effects of the material to be machined, cutting tool and cutting process are reflected in the cutting force. Taylor proposed three distinct models to predict specific cutting energy during machining of grey cast iron, white cast iron and mild carbon steel. The first two models are defined as function of feed per tooth and depth of cut. In the last one, the effect of depth of cut was not considered. ASME and AWF proposed prediction models of specific cutting energy in which the type of material to be machined is considered by means of a material constant. It must be noted that these material

constants were established under experimentation considering some specific characteristics of the cutting tools (turning inserts). As in the model established by Taylor for mild carbon steel, depth of cut does not affect specific cutting energy. Additionally, Dormer proposed a model specified for milling operations in which the effect of depth of cut was disregarded once more.

In all the aforementioned models (disregarding the model proposed by Taylor for cast irons), the effects of depth of cut and cutting speed were not included, which may not be valid in general. The fact that a parameter is not significant during a certain machining operation does not imply that it will not be significant for a different machining operation. Furthermore, some models were established under particular factors, such as the characteristics of the cutting tools used by ASME and AWF, which suggests that these models were defined during turning experiments. However, when performing operations with different cutting tools, or when the models are used to estimate the specific cutting energy for processes different from those considered during its formulation, the accuracy of the models may be compromised. These gaps lead to lack of compliance between the models and thus the actual specific cutting energy, suggesting that these models should not be used for any material, cutting tool and cutting process. As a consequence, specific cutting energy cannot be estimated as reliable as possible. This responds to the objective of the dissertation, that is the development of a methodology that permits to formulate a model of specific cutting energy, similar to those presented in this sub-chapter and appropriate for a particular cutting process, cutting tool and material.

3

METHODOLOGY

3.1 Introduction

The aim of the present dissertation is to create a comprehensive step-by-step methodology from which a practical model of specific cutting energy can be formulated. Firstly, to achieve this purpose, a statistical analysis is carried out for a better comprehension of the process. Through this analysis, performed using DoE, ANOVA and RSM, the cutting parameters whose effect is statistically significant for the specific cutting energy are identified and an expression of the response surface, dependent on these parameters, is obtained. However, in terms of process planning, this model is not adequate to estimate the specific cutting energy. Instead, it allows to acquire an idea of the overall system behaviour within a certain experimental range, quantifying the correlation between the parameters and this indicator. Thus, after conducting this preliminary statistical study, as a result of the obtained results, another specific cutting energy model, similar to those pointed in chapter 2.2.5.2, is proposed.

The following sub-chapters present an overview related to DoE, ANOVA and RSM.

3.1.1 Design of Experiments

An experiment can be defined as a series of controllable tests, where intentional changes are made to the input variables of a system, to evaluate the influence that they have on the final response of the system. DoE refers to the process of planning the experiment in order to collect appropriate data, so that valid and objective conclusions can be drawn by means of statistical approaches [26]. The application of DoE technique allows to maximise the amount of

information obtained through a reduced number of experimental trials, with the aim of identify the main inputs of the system and describe the process behaviour in a specific domain through a mathematical model.

For that purpose, the desirable final response and the factors presumed to influence the performance of the process must be clearly identified. Then, through an adequate experimental design, which ultimately depends on the objectives of the experiment and the number of factors to be investigated [27], the impact of each factor on the final response of the system subjected to evaluation is statistically determined. Notwithstanding this, the understanding of the process fundamentals must not be ignored. Table 3.1 shows the guidelines for designing experiments proposed by Montgomery.

Table 3.1 Guidelines for designing an experiment [26]

1. Recognition and statement of the problem	Pre-experimental planning
2. Choice of factors, levels, and ranges [a]	
3. Selection of the response variable [a]	
4. Choice of experimental design	
5. Performing the experiment	
6. Statistical analysis of the data	
7. Conclusions and recommendations	

[a] In practice, steps 2 and 3 are often done simultaneously or in reverse order.

3.1.2 Analysis of Variance

ANOVA is one of the most widely used statistical methods to analyse scientific experiments. This method is often used to examine the significance of factors in a multi-factor experiment [8]. In general, the ANOVA technique involves sum of squares (SS), degrees of freedom (DF), mean square (MS), *F-value* and *p-value* (Prob $>$ *F*) for all the factors. SS is the sum of squared deviations from the mean while MS is the variance associated with each term whose value is calculated by dividing SS by DF [14]. The statistics test for the ANOVA is an *F*-test, in which the test statistic is considered to follow an *F*-distribution under the null hypothesis [8]. This test is used with the purpose of determine whether a particular term is associated with the response or not. The *F-value* for a particular factor is obtained by the ratio

between MS for that term and MS for the residual. The probability that a term is modelling noise rather than serving to explain the trend is expressed by the value of Prob $> F$ [14].

3.1.3 Response Surface Methodology

Several experimental programs are designed with a two-fold purpose in mind: to quantify the relationship between the values of some measurable response variable(s) and those of a set of experimental factors presumed to influence the response(s) and, to find the values of the factors that lead to the optimum value or values of the response(s) [28].

RSM consists of a set of techniques used in the empirical study of the relationships between one or more responses and a group of input variables, and the objective is to optimise those responses [26] or, at least, gain a better understanding of the overall response system [28]. This technique focuses on quantify the relationship between the values of the measurable response variable(s) (dependent variables) and the values of the factors that may possibly influence the response variable(s) (independent variables), through a regression analysis.

In a regression analysis, the data are obtained from an experimental procedure and then used to express the correlation between the response variable(s) and the factors presumed to affect the response(s), through a mathematical model. Usually, the correlation between the response and the factors is unknown. In most cases, a second-order model, given by Equation (3.1) [28], is adequate to fit a response, in which Y is the response, k is the number of factors, x_i and x_j are the levels of the factors, β_i are the regression coefficients for the first-degree terms, β_{ii} are the coefficients for the pure quadratic terms, β_{ij} are the coefficients for the cross-product terms and ε is the experimental error. The total number of coefficients in the response polynomial, $n\beta$, is obtained through Equation (3.2).

$$Y = \beta_0 + \sum_{i=1}^{k} \beta_i x_i + \sum_{i=1}^{k} \beta_{ii} {x_i}^2 + \sum_{i=1}^{k} \sum_{j>i}^{k} \beta_{ij} x_i x_j + \varepsilon \quad \textbf{(3.1)}$$

$$n\beta = (k+1) \cdot \frac{k \cdot (k+1)}{2} \quad \textbf{(3.2)}$$

3.1.3.1 Central Composite Design

Central Composite Design (CCD) is one of the most widely used designs for fitting a second-order model. Generally, the CCD consists of a 2^k factorial design, that is, a design with k factors each at two levels, with n_F factorial runs ($n_F = 2^k$), $2k$ axial or star runs and n_C center runs. Equation (3.3) gives the total number of experiments needed to perform a CCD plan.

$$N = n_F + 2k + n_C \tag{3.3}$$

The n_F factorial points correspond to the vertices of a regular polygon in a plane ($k = 2$), a polyhedron in a three-dimensional space ($k = 3$), or a polytope in a higher-dimensional space ($k \geq 4$) [28], with coordinates $(x_1, x_2, \dots, x_k) = (\pm 1, \pm 1, \dots, \pm 1)$. The $2k$ axial points are the vertices of a k-dimensional star. For example, considering a CCD with three factors, the coordinates of the axial points will be $(\pm\alpha, 0,0)$, $(0, \pm\alpha, 0)$ and $(0,0, \pm\alpha)$. The n_C center points correspond to the design center, that is, the center of a circle ($k = 2$), the center of a sphere ($k = 3$) or the center of a hypersphere ($k \geq 4$) [28], with coordinates $(x_1, x_2, \dots, x_k) = (0,0, \dots, 0)$. Figure 3.1 schematizes the CCD with two and three factors.

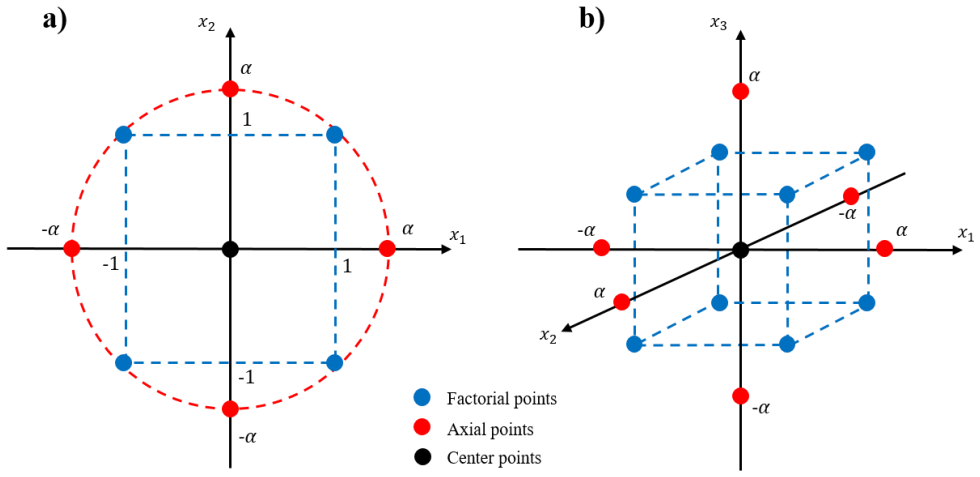

Figure 3.1 Central Composite Design: a) k = 2; b) k = 3

To apply the CCD, there are two parameters that must be specified, namely the distance α of the axial runs from the design center and the number of center points, n_C.

Box and Hunter [29] referred that a second-order response surface design should be rotatable. That means that the variance of the predicted response is the same at all points that are at the same distance from the design center. A CCD is made rotatable by the choice of α, which is dependent on the number of points in the factorial portion of the design, n_F, and it is given by Equation (3.4) [26]. Additionally, the design must include center runs to provide reasonably stable variance of predicted response. In general, three to five center runs are recommended [26].

$$\alpha = (n_F)^{\frac{1}{4}} \tag{3.4}$$

In order to combine values of different natures in the model, it is necessary to normalize the data using coded variables. Thus, each factor is varied in five coded levels: -α, -1, 0, +1 and +α, thus constituting an experimental range [-α, +α] for each cutting parameter. A real value of the factors is assigned to each coded variable.

3.2 Stages of the Methodology

In this dissertation, a proper methodology was defined and strictly followed, in order to acquire the appropriate data that lead to credible results and conclusions. The applied methodology is subdivided in six stages, namely:

- Stage I: Operation, material, cutting tool and experimental plan development;
- Stage II: Data acquisition procedure and specific cutting energy calculation;
- Stage III: Statistical analysis of the data and obtention of the response surface model;
- Stage IV: Specific cutting energy model for process planning;
- Stage V: Validation procedure of the specific cutting energy model for process planning;
- Stage VI: Comparative analysis between the validation tests and the estimates provided by other models.

The process begins with Stage I. This stage deals with the aspects that must be attended to before proceeding with the experiments. The machining process to be performed is defined,

the workpiece material and the cutting tool are chosen, the levels of the cutting parameters are established, and the experimental plan is developed in this stage.

This point determines the beginning of Stage II. In this stage, the necessary data to calculate specific cutting energy for each experiment, that is, the cutting forces measurements, is acquired through the execution of the experimental plan defined in Stage I.

Thereafter, in Stage III, ANOVA and RSM are applied to statistically evaluate and quantify the influence of each cutting parameter, namely feed per tooth, depth of cut and cutting speed, on specific cutting energy, for the combination cutting operation / material / cutting tool established in Stage I. As noticed before, the expression of the response surface is obtained in this stage.

The results obtained through Stage III will lead to a new series of more detailed experiments considering only the most influent factors identified in this stage. During Stage IV, the model intended to be formulated dependent on these significant cutting parameters is formulated.

Afterwards, Stage V consists in performing several experiments to prove the veracity of the model formulated previously. The aim is to verify if the estimates provided by the model are in accordance with the specific cutting energy calculations from the validation tests.

For last but not the least, the last stage of the methodology applied in this dissertation, Stage VI, consists of a comparative analysis between the results obtained in the validation tests and the estimates provided by the models identified in chapter 2.2.5.2 and the response surface model obtained through RSM technique. The main objective is to ascertain if the formulated model provides more accurate estimates than the other models. After this, the main conclusions can be drawn.

3.2.1 Stage I: Operation, material, cutting tool and experimental plan development

Figure 3.2 presents a flowchart describing the first stage of the methodology. The first step of Stage I consists in choosing the cutting operation to be performed, the workpiece material to be machined and the cutting tool to be used in the experiments. Once the cutting operation, workpiece material and cutting tool are chosen, the next step of Stage I is to establish

the levels of the cutting parameters, which are necessary for the development of the experimental plan.

The level 0 of each cutting parameter is assigned to the recommended value by the tool manufacturer. The experimental range is chosen to cover values around the recommendations provided by the tool manufacturer (levels -1 and +1), which are considered to be feasible to perform the experiments. The study domain is then extended to higher and lower values (levels $-\alpha$ and $+\alpha$) to analyse the global behaviour of the system.

Once established the levels of the cutting parameters, the experimental plan is developed.

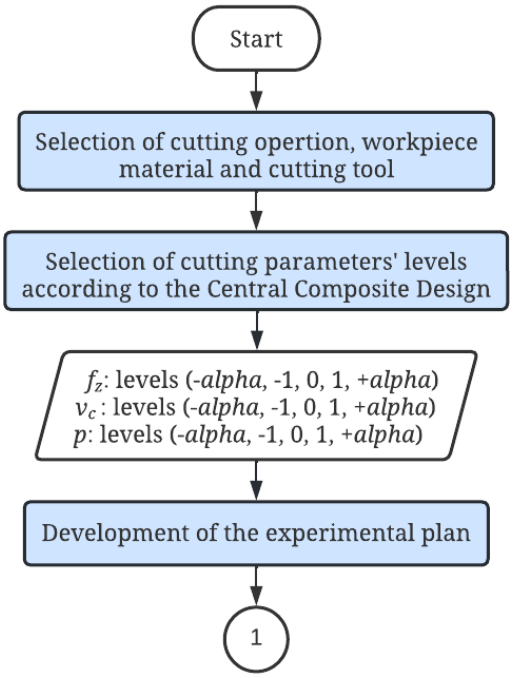

Figure 3.2 Flowchart describing Stage I

3.2.2 Stage II: Data acquisition procedure and specific cutting energy calculation

The flowchart of Stage II is depicted in Figure 3.3. Once the experimental plan is established, some tests must be carried out before performing the experiments in order to verify the correct force measuring by the device that acquires the data to calculate specific cutting energy. These preliminary tests are essential to ensure the accuracy and truthfulness of the final results.

The next step of Stage II is to conduct the experiments and obtain the measurements of the cutting forces for each experiment. Using *Matlab* software, the acquired data is treated and afterwards charts showing the evolution of the cutting forces during each experiment will be obtained. The cutting forces are not constant along the cutting process. For this reason, the obtained results must be analysed to understand the evolution of the cutting forces, to select the appropriate values that must be used to calculate specific cutting energy accurately. After the calculation of the cutting area, the specific cutting energy is obtained for each experimental trial through Equation (2.14), pointed in chapter 2.2.5.1.

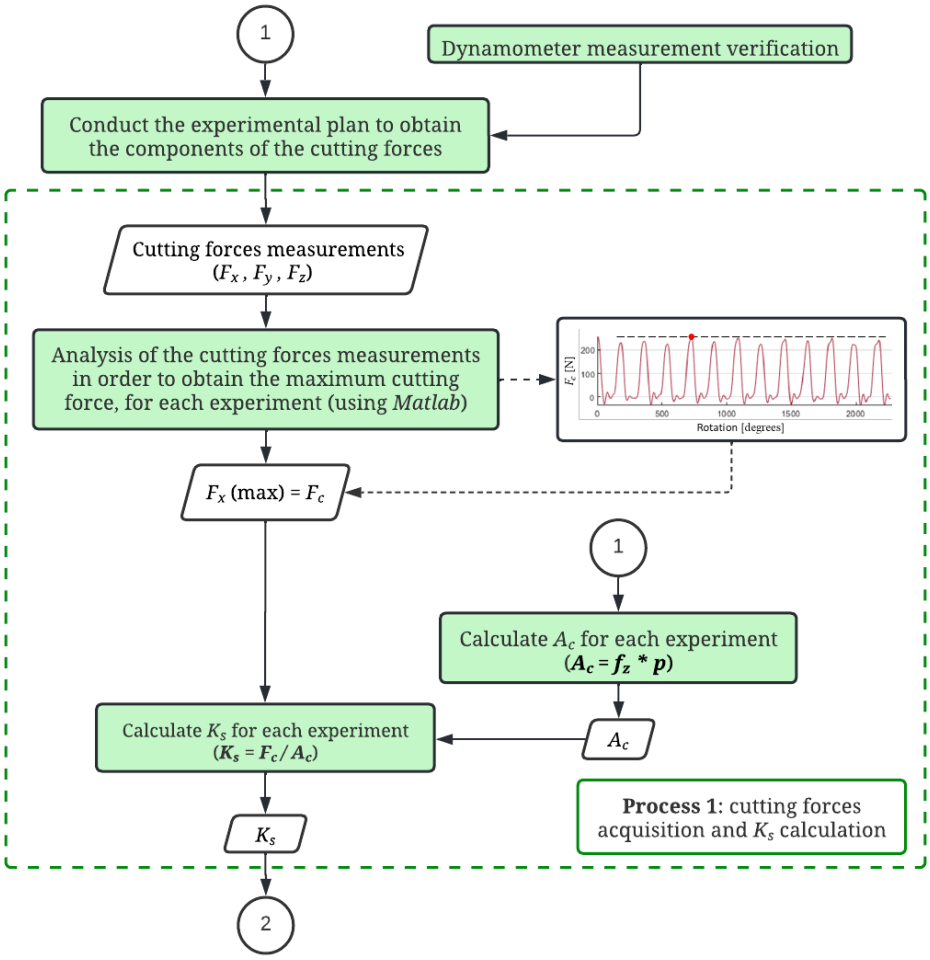

Figure 3.3 Flowchart describing Stage II

3.2.3 Stage III: Statistical analysis of the data and obtention of the response surface model

Figure 3.4 shows the descriptive flowchart of Stage III. After the estimation of specific cutting energy for each experiment, to prove the significance of each machining factor on this indicator, the influence ranking of the machining parameters (feed per tooth, depth of cut and cutting speed) will be obtained based on the ANOVA technique, using *Statistica* software [30]. If the *P-value* of a factor is smaller than α, the contribution of that factor is statistically significant, and vice-versa. After identified the factors whose contributions are statistically significant, the effects of the non-significant factors are ignored and the response surface model is obtained.

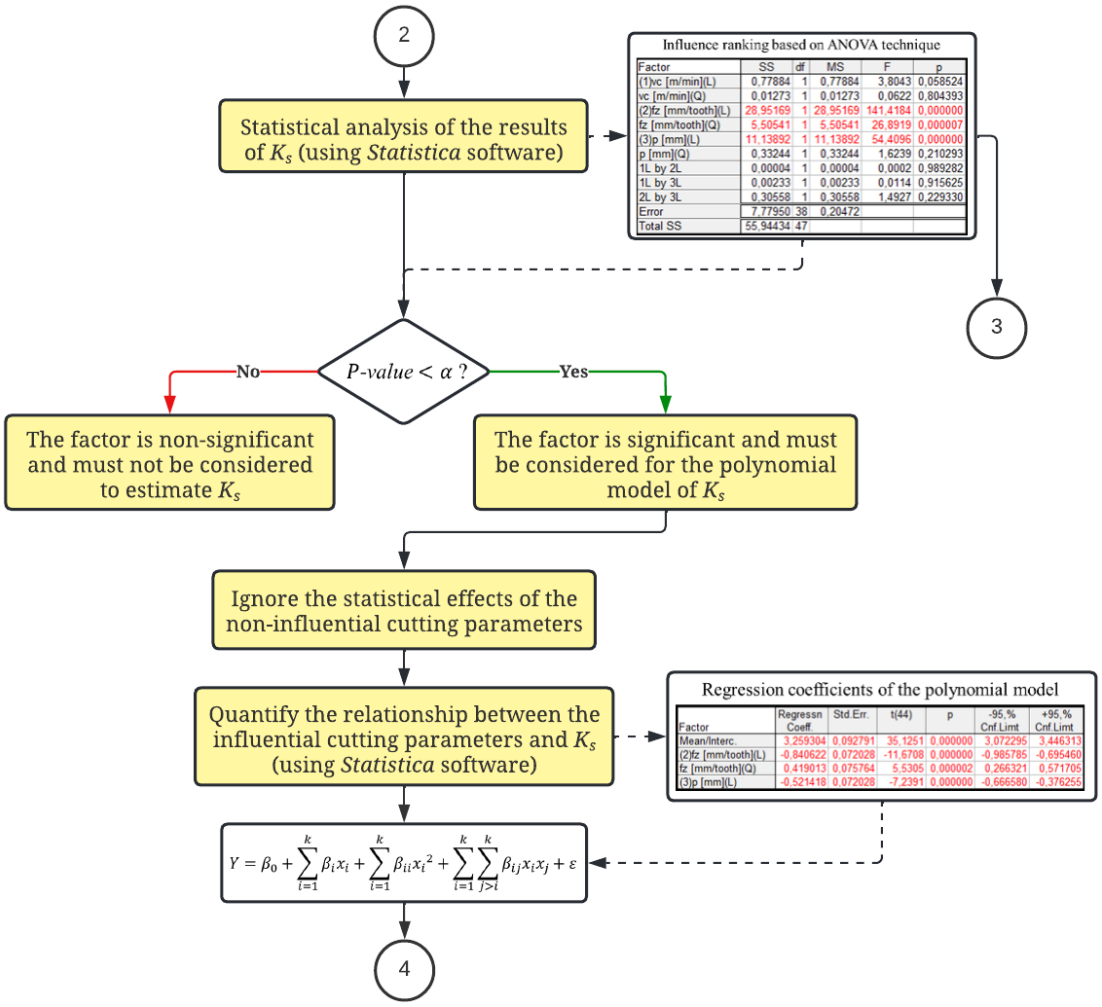

Figure 3.4 Flowchart describing Stage III

However, the response surface model is not adequate to estimate specific cutting energy in terms of process planning. This polynomial model is an expression of the response surface, which is a powerful tool for exploring the relevance of variables and application domains, but not appropriate to predict that response in a practical way.

Thus, the results obtained from ANOVA and RSM will constitute the basis for a new more detailed experimentation (Stage IV), allowing to create a simple and more practical model to estimate the specific cutting energy.

3.2.4 Stage IV: Specific cutting energy model for process planning

Figure 3.5 presents the flowchart related to the fourth stage of the methodology. Firstly, the ANOVA results obtained previously in Stage III must be analysed, in order to establish a new appropriate series of experiments. The cross effects between the meaningful factors are decisive for this analysis. If the cross effects are statistically significant, thus indicating that the effect of one cutting parameter is affected by other(s), the response surface model obtained using RSM technique must be used to estimate specific cutting energy. Ultimately, a new study must be performed regarding this question. However, if the cross effects are not statistically significant, it means that the effect of one cutting parameter is not affected by other parameters. Thus, if there is more than one statistically significant cutting parameter, one of them can be varied while keeping the other(s) constant.

In Stage I, experimental ranges [$-\alpha$, $+\alpha$] were defined for each cutting parameter with the purpose of analysing the response system over an extended domain. However, the correspondent values of the extreme levels of these ranges (levels $-\alpha$ and $+\alpha$) are distinct from the tool manufacturer´s recommendations and consequently should not be used in practice to perform a cutting operation. Due to this fact, and with the aim of obtaining a specific cutting energy model applicable to a range of more feasible cutting parameters values, the extreme values of each parameter were disregarded for the next procedure.

Afterwards, new values are established for each cutting parameter whose contributions were statistically significant for specific cutting energy and a new experimental plan is developed. By comparison, the upper and lower values of the new experimental ranges correspond to levels -1 and +1 considered before in the CCD plan, whose corresponding values are close to the recommendations of the tool manufacturer. From the new set of experiments,

independent specific cutting energy expressions as function of each influent machining parameter are obtained, which subsequently are combined to create a single model to estimate specific cutting energy.

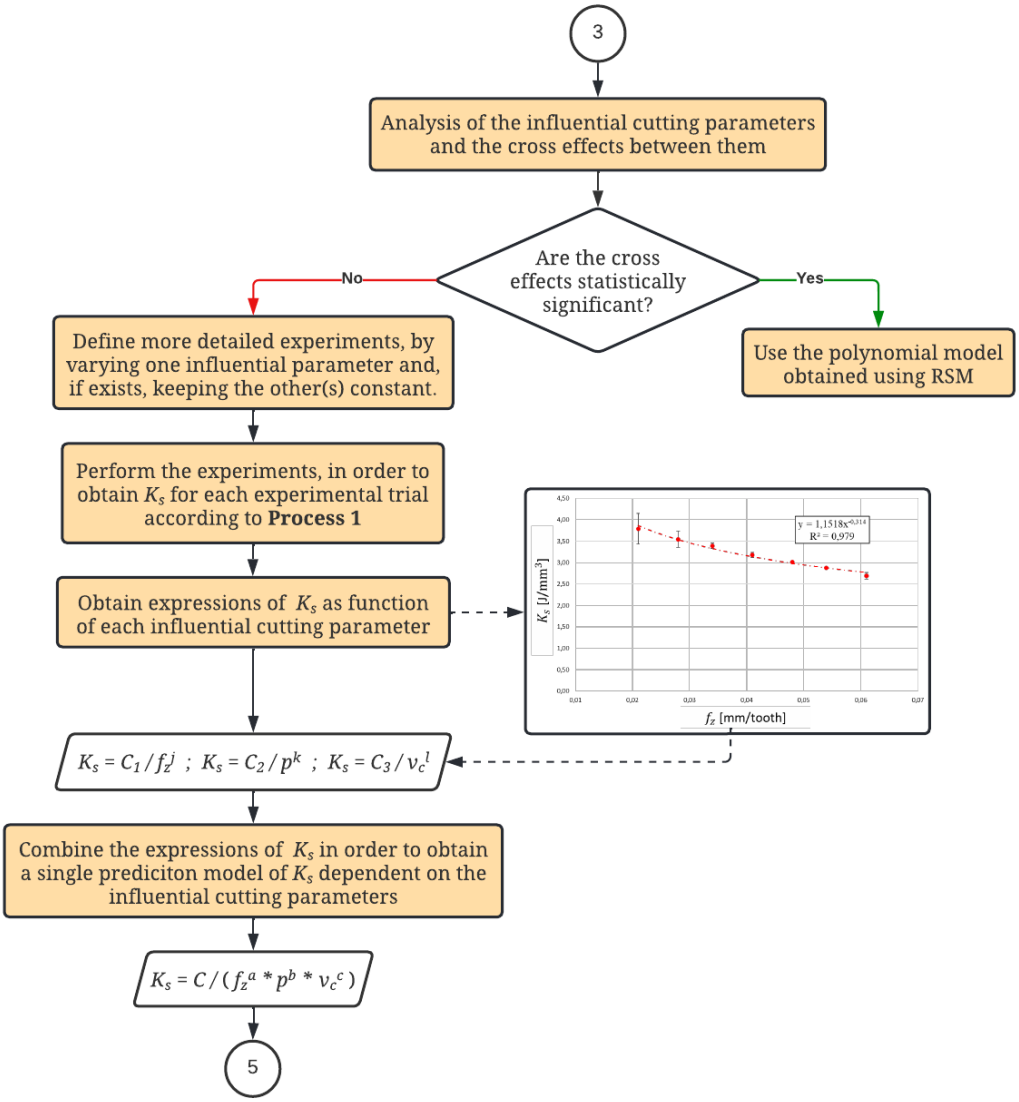

Figure 3.5 Flowchart describing Stage IV

3.2.5 Stage V: Validation procedure of the specific cutting energy model for process planning

Figure 3.6 depicts an auxiliary flowchart defining the necessary inputs for the validation procedure, which is presented in Figure 3.7. The first step of Stage V is to define several validation tests, by varying the cutting parameters randomly within the practicable ranges

defined previously in Stage IV. The validation tests must be conducted in order to calculate specific cutting energy for each validation test, as described by Process 1.

The validation procedure consists of estimating the specific cutting energy according to the model formulated, for the same combinations of cutting parameters considered in the validation tests, as shown in Figure 3.6. Afterwards, the relative error between the estimates provided by the model and the experimental results obtained from the validation tests is calculated, with respect to the experimental results, as presented by Equation (3.5).

$$Error = \frac{K_s\ (model) - K_s\ (experimental)}{K_s\ (experimental)} \cdot 100 \quad \textbf{(3.5)}$$

Then, in reverse, once created a specific cutting energy model as function of the cutting parameters, it is possible to estimate the cutting forces inherent to the milling operation through Equation (2.14), presented before in chapter 2.2.5.1. Therefore, using the estimates provided by the model, the cutting forces are afterwards calculated. Next, although the result is redundant, the estimated cutting forces are compared to the experimental values, i.e. the cutting forces measured by the dynamometer during the validation tests, by calculating the relative error between them. As previously, the error is calculated in relation to the experimental results, as shown in Equation (3.6).

$$Error = \frac{F_c\ (model) - F_c\ (experimental)}{F_c\ (experimental)} \cdot 100 \quad \textbf{(3.6)}$$

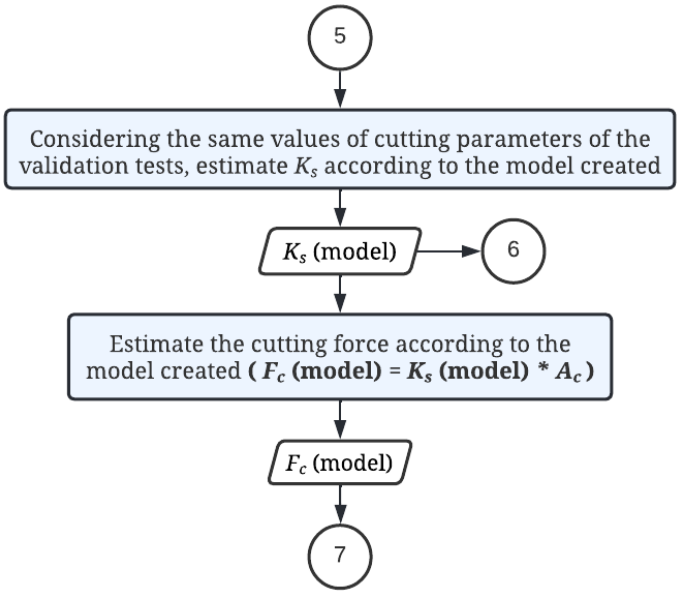

Figure 3.6 Auxiliary flowchart of Stage V

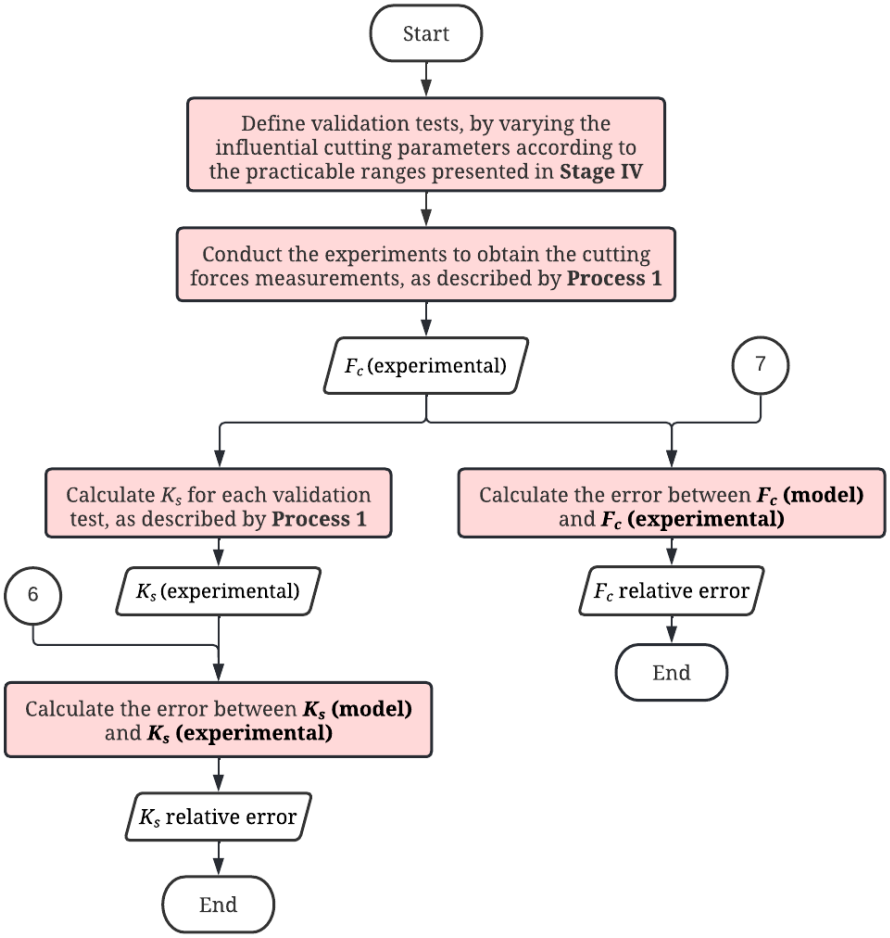

Figure 3.7 Flowchart describing Stage V

3.2.6 Stage VI: Comparative analysis between the validation tests and the estimates provided by other models

Figure 3.8 shows the descriptive flowchart of Stage VI. The last stage of the applied methodology consists in a comparative analysis between the experimental results from the validation tests and the estimates provided by other empirical models. Ultimately, it enables to analyse how accurate the model formulated is in relation to other models.

For this purpose, considering once again the same combinations of cutting parameters used for the validation tests, the specific cutting energy is estimated according to the models proposed by ASME, AWF, Taylor, Dormer and the response surface model. Further, the estimates provided by the models are compared to the experimental results from the validation tests, by calculating the relative error between the results in relation to the experimental ones, through Equation (3.7). Finally, based on the results obtained, the main conclusions can be drawn.

$$Error = \frac{K_s\ (other\ models) - K_s\ (experimental)}{K_s\ (experimental)} \cdot 100 \qquad \textbf{(3.7)}$$

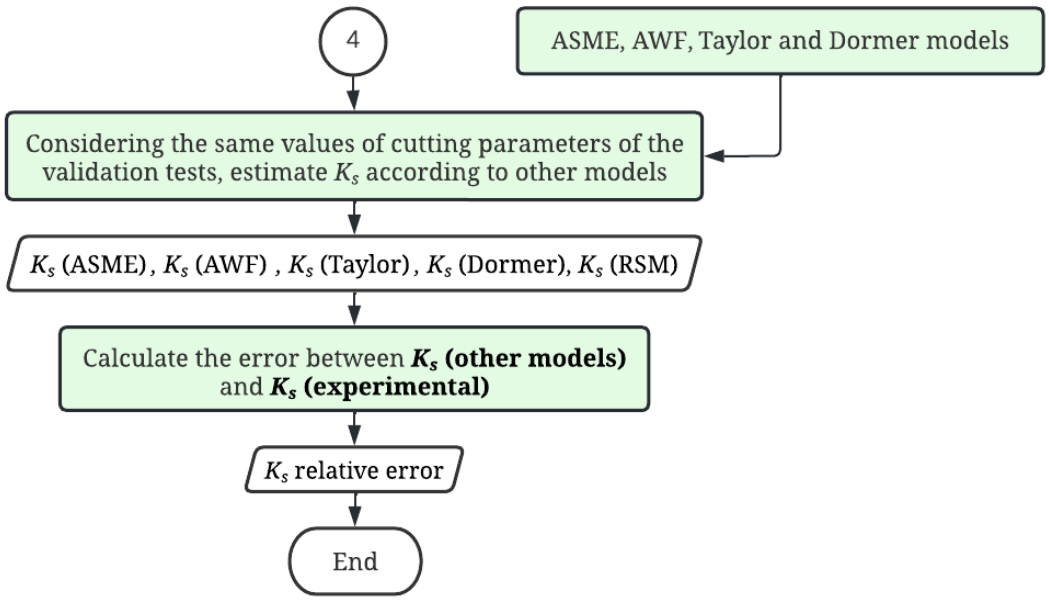

Figure 3.8 Flowchart describing Stage VI

4

EXPERIMENTAL PROCEDURE

4.1 Introduction

In the present chapter, a comprehensive description related to the experimental procedure adopted in this dissertation is made. Firstly, the experimental setup for collecting the necessary data is presented. Next, the main characteristics of the machine tool used to perform the cutting operations are shown. Subsequently, the specifications of the workpiece material to be machined and the characteristics of the cutting tool used in the experiments are addressed. The cutting parameters recommended by the tool manufacturer for the machining pair material/cutting tool are also shown in this section. Afterwards, the process of cutting forces acquisition is fully detailed to completely understand how the experimental data is acquired. For last, the preliminary verification tests and the experimental plan defined according to the CCD are presented.

4.2 Experimental Setup

The experimental setup used in this research, presented in Figure 4.1 and schematized in Figure 4.2, allows to acquire the cutting forces that will be used to calculate the specific cutting energy for each experimental trial.

The sample to be machined was fixed to the fixture system, which is screwed to the dynamometer. On the other hand, the dynamometer is screwed to a base plate which in turn is screwed to the CNC table. During the cutting process, the signal from the dynamometer is processed by a charge amplifier and data acquisition (DAQ) system. Afterwards, the signal is

converted into the three components of the resultant force inherent to the milling process, enabling to calculate the specific cutting energy for each experiment. In the following sub-chapters, the machine tool, workpiece material and cutting tool are addressed.

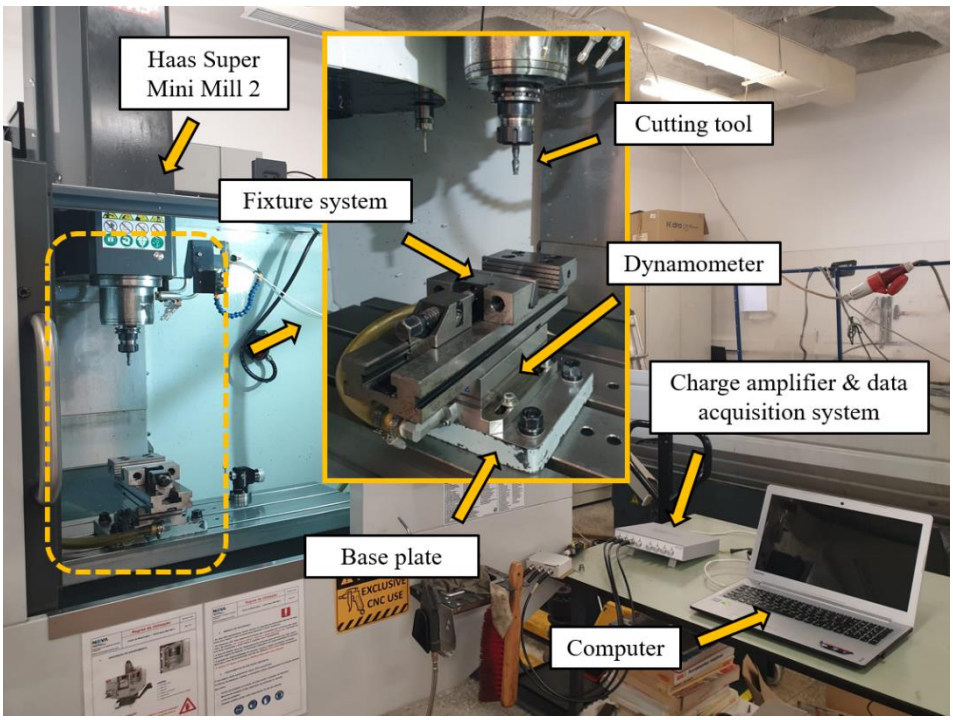

Figure 4.1 Experimental setup

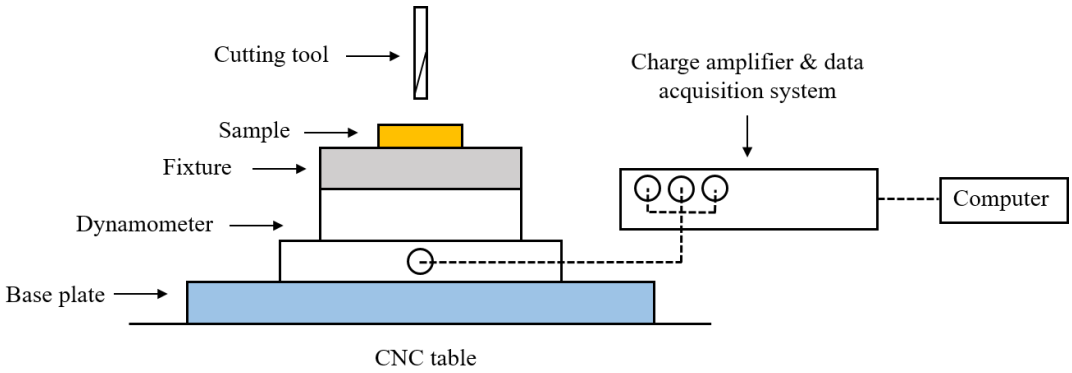

Figure 4.2 Schematic representation of the experimental setup

4.2.1 Machine tool

All experimental work for this study was performed on a Haas Super Mini Mill 2 CNC machine with three axes (Figure 4.3), present in the Department of Mechanical and Industrial Engineering Laboratory of Nova School of Science and Technology. The main characteristics of the machine tool are summarized in Table 4.1.

Figure 4.3 Haas Super Mini Mill 2 [31]

Table 4.1 Main characteristics of Haas Super Mini Mill 2 [31]

Max. power [kW]	Max. speed [min^{-1}]	Max. Torque [Nm]	Axis	Tool capacity
11.2	10000	23 @ 4600 min^{-1}	3	20

4.2.2 Workpiece material

The material used in the experiments was 1.2738 HH tool steel (W-NR standard). This alloy steel can be used for hot or cold working and it is characterized by its high hardness and toughness promoted by the content of the elements nickel, chromium and molybdenum. It is suitable for applications demanding wear resistance, including plastic moulds, casting dies, stamping tools, hydroforming tools, shafts and gears. In fact, this steel is one of the most widely

used materials in the mould industry. To produce a mould cavity, large quantities of material must be removed, which consequently leads to a high energy consumption. Therefore, the use of the steel as base material in this research work generates an additional source of knowledge for this type of industry in particular. Tables 4.2 - 4.4 present the chemical composition, physical and mechanical properties of 1.2738 HH tool steel, respectively.

Table 4.2 Chemical composition of 1.2738 HH tool steel [32]

Element	**C**	**Si**	**Mn**	**P**	**S**	**Cr**	**Mo**	**Ni**
%	0.40	0.30	1.50	≤ 0.01	≤ 0.01	1.90	0.20	1

Table 4.3 Physical properties of 1.2738 HH tool steel [32]

Density [kg/m^3]	**Thermal expansion coefficient [10^{-6} m/m^{o}C]**	**Thermal conductivity [W/mK]**
	20 – 200 ^{o}C	**20 ^{o}C**
7.80	12.70	29

Table 4.4 Mechanical properties of 1.2738 HH tool steel [32]

Hardness [HB]	**Modulus of Elasticity [GPa]**	**Yield strength [MPa]**	**Tensile strength [MPa]**
300	205	826	993

To ensure the material identity, hardness experiments were conducted on a Mitutoyo HM – 112 Micro – Vickers Hardness Testing Machine, following the ASTM E384 technical directive for Microindentation Hardness of Materials. Figure 4.4 depicts the hardness measurements along the sample. The average value was calculated from the registered measurements and is equal to 330 HV, which approximately corresponds to 314 HB, slightly higher than the reference value pointed in Table 4.4.

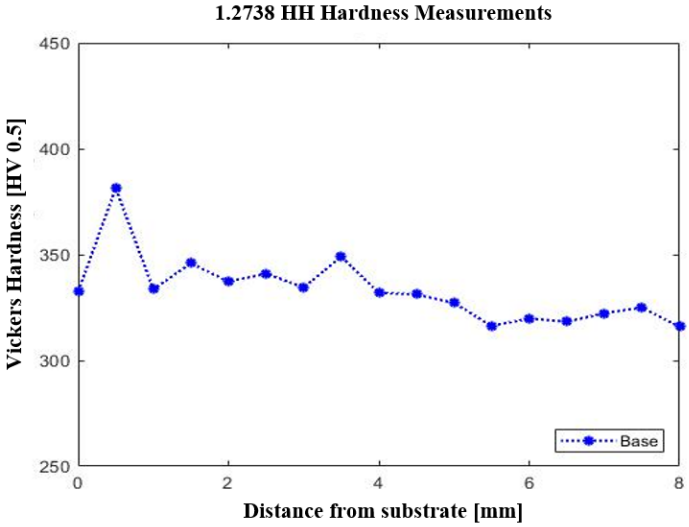

Figure 4.4 Vickers hardness tests for 1.2738 HH tool steel

4.2.3 Cutting tool

The cutting tool used in the experimental work was a coated solid carbide end mill S710 from Dormer (Figure 4.5). A coated mill was chosen due to the high number of experiments needed to address the final results initially established. The coating promotes a slower tool wear when compared to uncoated mills, thus increasing tool life. The main characteristics of the cutting tool are summarized in Table 4.5. According to the workpiece material to be machined, the cutting parameters recommended by Dormer for this cutting tool were registered and pointed in Table 4.6.

Figure 4.5 S710 end mill [25]

Table 4.5 Main characteristics of S710 end mill [25]

Diameter [mm]	Helix angle [º]	Cutting edges	Coating
10	40	2	AlCrN

Table 4.6 Cutting parameters recommended by Dormer for S710 end mill [25]

Material	f_z [mm/tooth]	v_c [m/min]	p [mm]
1.2738 HH	0.041	120	5 (max)

4.3 Cutting Forces Acquisition

To calculate specific cutting energy, it is necessary to measure the cutting forces inherent to the milling process. A Kistler 9257B dynamometer and a Kistler LabAmp 5165A charge amplifier & DAQ system for dynamic measurements were used to measure the components of the cutting force during the milling process.

The multicomponent Kistler 9257B dynamometer (Figure 4.6) enables an accurate measurement of highly dynamic forces. The device, used for measuring the three orthogonal components of the resultant force, consists of four three-component force piezoelectric sensors fitted under high preload between a baseplate and a top plate. Each sensor contains three pairs of quartz plates, one sensitive to pressure in the z direction and the other two responding to shear in the x and y directions, respectively [33]. To ensure the quality of the acquired data, the measurement axes of the dynamometer (x, y and z) were aligned with the axes of the CNC machine, using a dial indicator. The main characteristics of the dynamometer are summarized in Table 4.7.

Table 4.7 Main characteristics of Kistler 9257B dynamometer

Characteristics	
Range [kN]	F_x, F_y: -5 – 5 / F_z: -5 – 10
Sensivity [pC/N]	F_x, F_y: -7.5 / F_z: -3.7

The Kistler 9257B dynamometer is connected directly to the measuring channels of Kistler LabAmp 5165A charge amplifier & DAQ (Figure 4.7). Each channel allows to measure a component of the resultant force: channel one, two and three measure F_x, F_y and F_z components, respectively. Piezoelectric sensors, present in the dynamometer, produce an electric charge which varies in direct proportion with the load acting on the sensors [33]. Then, the amplifier converts this charge directly into digital values, given in [N].

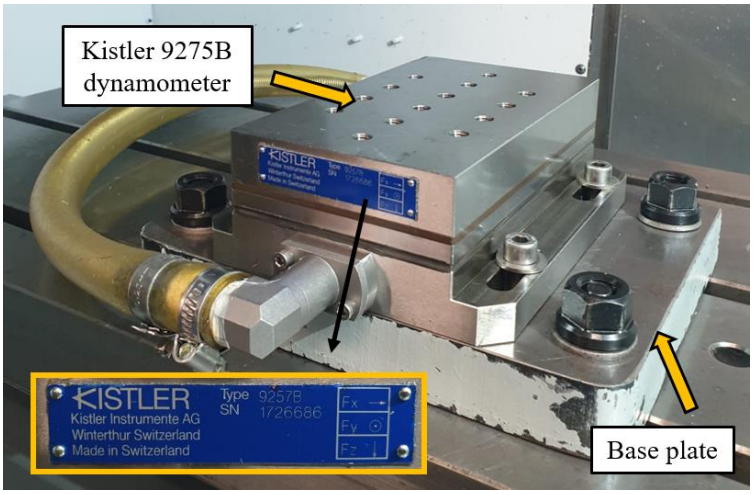

Figure 4.6 Kistler 9257B dynamometer

Figure 4.7 Kistler LabAmp 5165A charge amplifier & DAQ

The device has an integrated DAQ system, which allows to capture the signal. In the DAQ system interface, it is possible to define the sampling rate, the data acquisition time limit and the type of filter to be used. Due to the complexity of the cutting process, a sampling rate of 10 kHz was set. To ensure a representative reading of the values, a time limit of 5 minutes per experiment was set to acquire all the data needed. The data acquisition was started and stopped manually, at the beginning and at the end of each experiment, respectively. During the data acquisition procedure, no filter was used. As there is a web server running on the device, the data is acquired by connecting the LabAmp to a computer via a network cable. Afterwards, the computer generates a .csv file with the raw data acquired during the experiment.

Afterwards, *MatLab* software was used to develop a routine to process and analyse the .csv file with the acquired raw data. A butterworth low pass filter was used to supress interfering

signals and reduce background noise due to the machining center, the electrical installation or the equipment used. Through this program, the evolution of the cutting forces along each milling experiment was obtained.

As mentioned previously in chapter 2.2.4, the resultant force that acts at the tip of the cutting edge, F_R, can be decomposed in two components: the active force, F_{ac}, and the passive force, F_p. In turn, the active force is decomposed in two other components: the support force, F_s, oriented perpendicularly to feed direction, and the feed force, F_f, oriented according to the feed direction. By observing Figure 4.8, it can be noted that the three components F_s, F_f and F_p are aligned with the dynamometer measurement axes *x*, *y* and *z*, respectively.

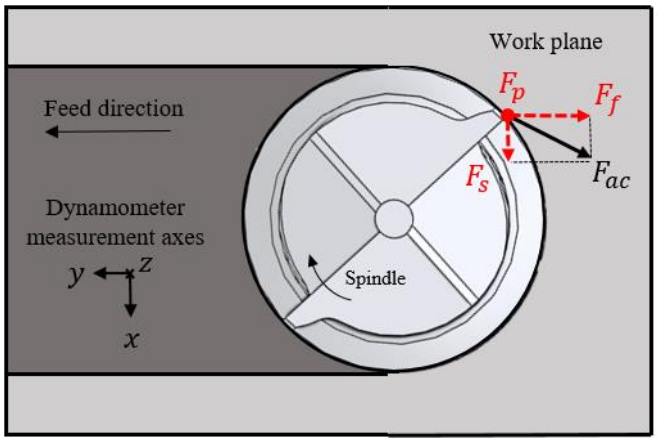

Figure 4.8 Components of the resultant force acting at the reference point of the cutting edge

It was also noticed that, when the angle φ between the cutting direction and feed direction is equal to 90º, the support force corresponds to the cutting force, F_c, which is the exact force measured in the x direction, according to the dynamometer measurement axes (Figure 4.9). Moreover, when $\varphi = 90º$, the cutting area reaches its maximum value, which implies that the maximum cutting force, used to calculate the specific cutting energy, occurs at this point. Thus, for each experiment, the maximum force measured in the *x* direction will be registered and further used to calculate the specific cutting energy.

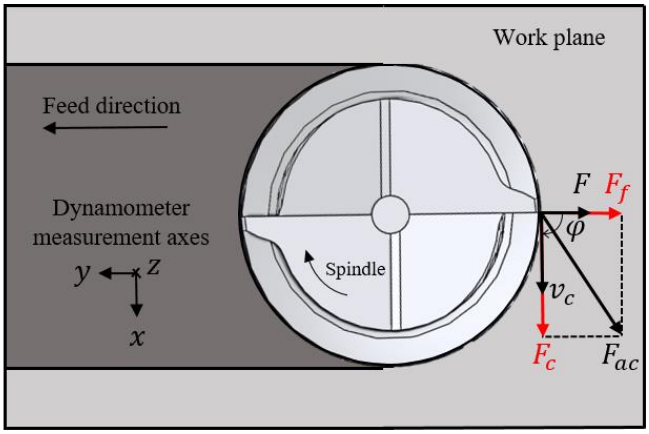

Figure 4.9 Components of the active force when $\varphi = 90^{o}$

4.4 Preliminary Tests

As described in chapter 3.2.2, some preliminary tests were carried out in order to ensure the quality of the data that will be acquired throughout this research work. During this study, the specific cutting energy was calculated from the cutting forces measured during each experiment using a Kistler dynamometer. Thus, it is extremely important to verify if the cutting forces measured by the equipment correspond to the reality, in order to guarantee correct specific cutting energy calculations.

To achieve this, a series of controllable measurements was carried out. Three distinct loads – a) 2 kg, b) 4 kg and c) 6 kg – were applied through the CNC control system in the x direction, since this is the direction according to which the cutting forces will be recorded to calculate the specific cutting energy. Each load was applied three times and afterwards plotted against the measurements made by the Kistler dynamometer. The obtained results are depicted in Figure 4.10 and summarized in Table 4.8. It can be noted that the force measurements registered by the Kistler dynamometer are in agreement with the applied load, thus suggesting that the Kistler equipment that will be used during the entire research work is acquiring reliable data.

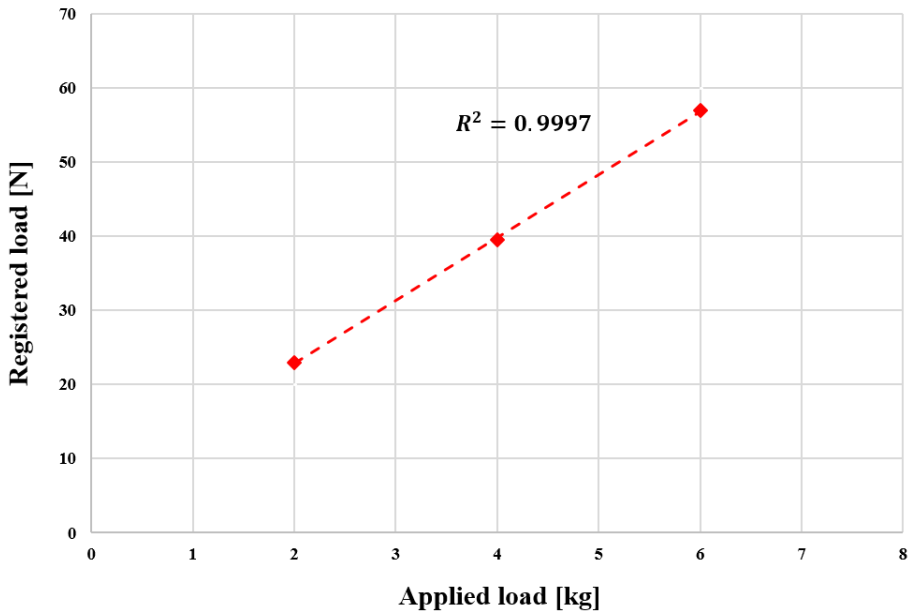

Figure 4.10 Kistler dynamometer measurements

Table 4.8 Results of the preliminary experiments

Preliminary experiment	Applied load [kg]	Kistler dynamometer measurements [N]	Average [N]
#PE1	2	22.8	23.0
#PE2		22.0	
#PE3		24.1	
#PE4	4	37.5	39.5
#PE5		40.4	
#PE6		40.5	
#PE7	6	55.3	56.9
#PE8		56.3	
#PE9		59.1	

4.5 Experimental Plan According to the CCD

The experimental planning consists in a 2^k full factorial design with 3 factors (k=3), 6 axial runs ($2k$ = 6) and 2 center runs ($n_c = 2$). The plan was replicated twice, for a total of 48 experimental trials. Table 4.9 presents the factors and their levels. The CCD experimental plan is depicted in Table 4.10.

Table 4.9 Factors and their levels

Levels (in coded variables)	**Factors**		
	v_c [m/min]	**f_z [mm/tooth]**	**p [mm]**
-1.68	100.00	0.007	1.00
-1	108.10	0.021	1.81
0	120.00	0.041	3.00
1	131.91	0.061	4.19
1.68	140.00	0.075	5.00

Table 4.10 CCD experimental plan

Run	Factors (in coded variables)		
	v_c	f_z	p
#1 / #17 / #33	-1	-1	-1
#2 / #18 / #34	-1	-1	1
#3 / #19 / #35	-1	1	-1
#4 / #20 / #36	-1	1	1
#5 / #21 / #37	1	-1	-1
#6 / #22 / #38	1	-1	1
#7 / #23 / #39	1	1	-1
#8 / #24 / #40	1	1	1
#9 / #25 / #41	-1.68	0	0
#10 / #26 / #42	1.68	0	0
#11 / #27 / #43	0	-1.68	0
#12 / #28 / #44	0	1.68	0
#13 / #29 / #45	0	0	-1.68
#14 / #30 / #46	0	0	1.68
#15 / #31 / #47	0	0	0
#16 / #32 / #48	0	0	0

5

RESULTS AND DISCUSSION

5.1 Introduction

The present chapter concerns about presenting, in a sequential way, the results derived from the experimental procedure described in chapter 4. Furthermore, a detailed interpretation of the acquired results is presented.

Firstly, after the execution of the CCD experimental plan, the evolution of the three components of the resultant force during each experimental trial, obtained using *Matlab* software, is interpreted, in order to understand the process dynamics and determine which cutting force value must be considered for the calculation of the specific cutting energy.

Subsequently, using *Statistica* software, the results derived from the ANOVA and RSM techniques are presented. In this phase, the influence of each cutting parameter on specific cutting energy is assessed, and the response surface model that quantifies that influence is pointed out.

Further ahead in this chapter, after identifying the key parameters, a new series of experimental tests is introduced in order to obtain independent specific cutting energy expressions dependent on each influential cutting parameter. The process of its combination, in order to achieve a single model dependent on these parameters, is fully described.

Finally, the validation tests to be performed to validate the formulated model are addressed and the correspondent experimental results are compared to the estimates provided by the model, thus proving its consistency. Likewise, the specific cutting energy calculations derived from the validation tests are also subjected to a comparative analysis with the estimates

provided by other models, namely the ASME, AWF, Taylor, Dormer and the response surface models.

5.2 Analysis of the Cutting Force Measurements

After ensuring that the dynamometer measures the applied forces correctly, the experimental plan defined according to the CCD was conducted. In order to analyse the cutting forces during each experiment, a *Matlab* routine to treat the acquired data was created. The cutting forces are not constant during the cutting process, which implies a completely understanding of the process dynamics to determine the cutting force value that must be considered to calculate the specific cutting energy for each experiment. Therefore, a detailed analysis of the cutting forces becomes determinant.

Using *Matlab* software, charts showing the evolution of the cutting forces for each experiment, according to the three measurement directions, were obtained. An experimental trial was randomly selected to execute this in-depth analysis. Figure 5.1 shows the evolution of F_x, F_y and F_z related to run #18, according to Table 4.10 presented in chapter 4.5.

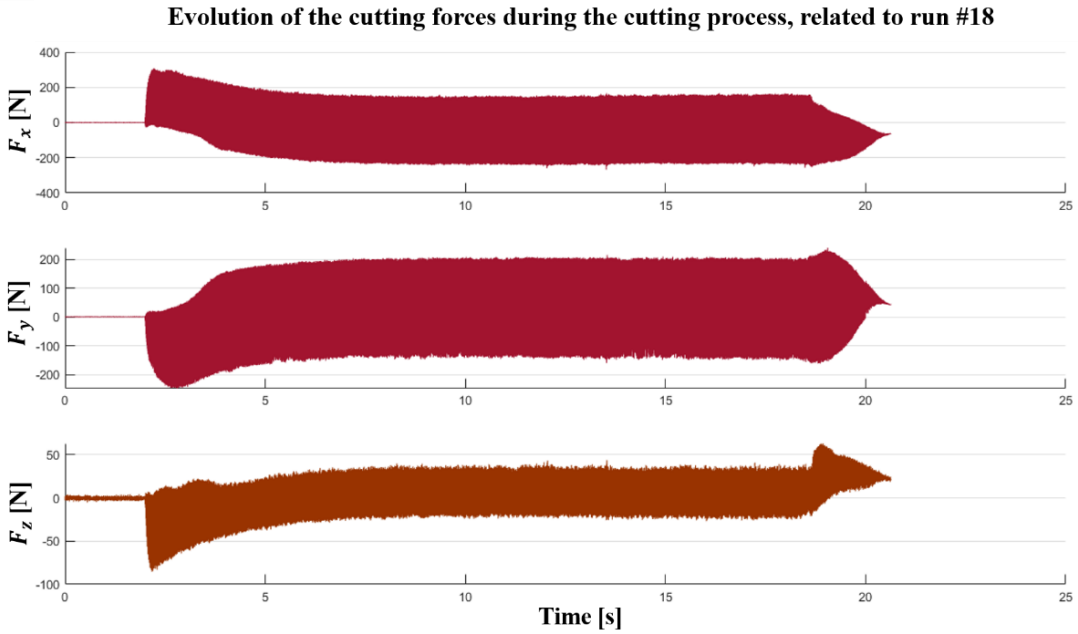

Figure 5.1 Evolution of the cutting forces relative to run #18

By observing Figure 5.1, it is explicitly noted that a stabilization of the evolution of the forces occur from five seconds on, which is not verified until that instant. At the beginning of the cutting process, F_x oscillates between a maximum positive value and approximately zero. As the process progresses, the force in the *x* direction starts to oscillate between positive and negative values, until it gets stabilized. The same trend can be observed in both charts relative to F_y and F_z. At this point, the main focus is directed towards the comprehension of this phenomenon.

In fact, the type of machining operation and the cutting tool used in the experiments are in the basis of this phenomenon. The end mill selected for the study has two cutting edges. At the beginning of the cutting operation, which consists in slot opening, only one cutting edge is effectively cutting the material at each instant. When one cutting edge stops to cut the material, only a few moments later the other cutting edge engages the workpiece (Figure 5.2a). Later, from the moment the cutting tool is half immersed in the part (Figure 5.2b), at first instance it may appear that, at the instant that one cutting edge engages the workpiece, the other one stops to cut the material. Thus, this fact suggests that during the entire process, only one cutting tooth is effectively cutting the part at each instant.

However, this statement is fallacious. Due to the helical geometry of the cutting edges (helix angle of 40º), there are some instants that both cutting edges are effectively cutting the material at the same time. Furthermore, as the tool approaches the position expressed in Figure 5.2b, the percentage of time during which both cutting edges simultaneously cut the material progressively increases. From the moment that the tool is half immersed in the part, this percentage of time remains constant, leading to a stabilization of the evolution of the forces.

Moreover, as depth of cut increases, the longer the time during which both cutting teeth are cutting at the same time (Figure 5.3). The red point marks the point where the front cutting edge stops cutting the material. Considering $p = 1$ mm (Figure 5.3a), the back cutting edge has already been cutting for t_1 seconds. However, if p = 2 mm (Figure 5.3b), the back cutting edge has already been cutting for t_2 seconds, with $t_2 > t_1$.

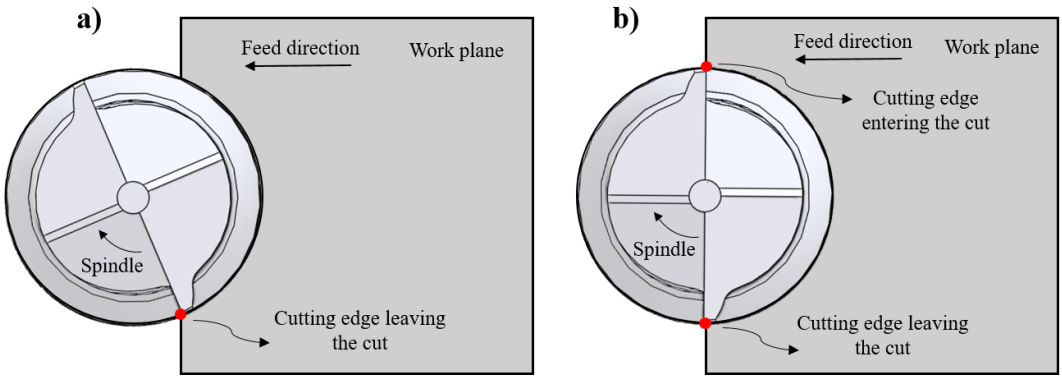

Figure 5.2 Slot milling operation showing where the cutting edges start and stop to cut the material: a) at the beginning of the cutting process; b) when the cutting tool is immersed in the workpiece at a distance equal to its radius

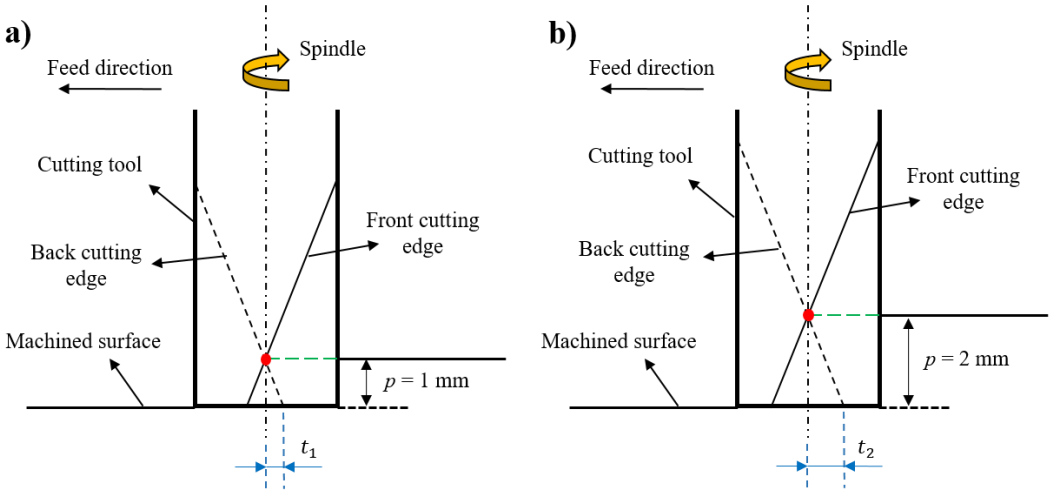

Figure 5.3 Both cutting edges cutting at the same time: a) for p = 1 mm; b) for p = 2 mm

Based on the machining parameters considered for run #18, the time it takes for the cutting tool to be immersed in the workpiece at a distance equal to its radius (as showed in Figure 5.2b) is exactly five seconds, which corresponds to the instant from which the evolution of the forces starts to stabilize in the charts. Thus, the fact that from this moment on two cutting edges start to cut the material simultaneously at some instants is at the origin of the evolution of the cutting forces observed previously in Figure 5.1.

For an in-depth analysis of the evolution of the forces, four analysis positions (A, B, C and D) were created (Figure 5.4). This detailed analysis will be made in relation to the rotation of the red cutting edge, hereinafter referred to as the reference cutting edge. Figures 5.5 and 5.6

depict a detailed view of the evolution of F_x, F_y and F_z, during a rotational period of the cutting tool, before and after the five seconds.

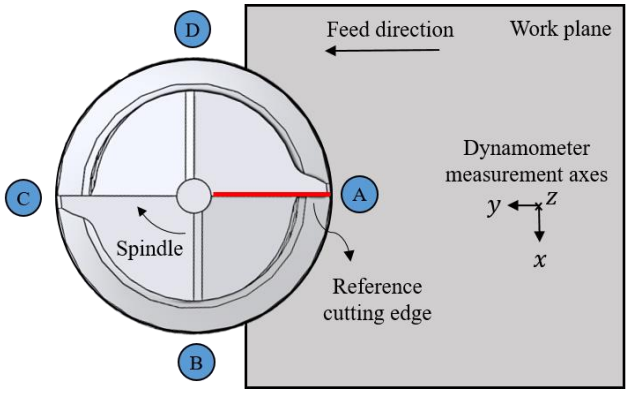

Figure 5.4 Analysis positions

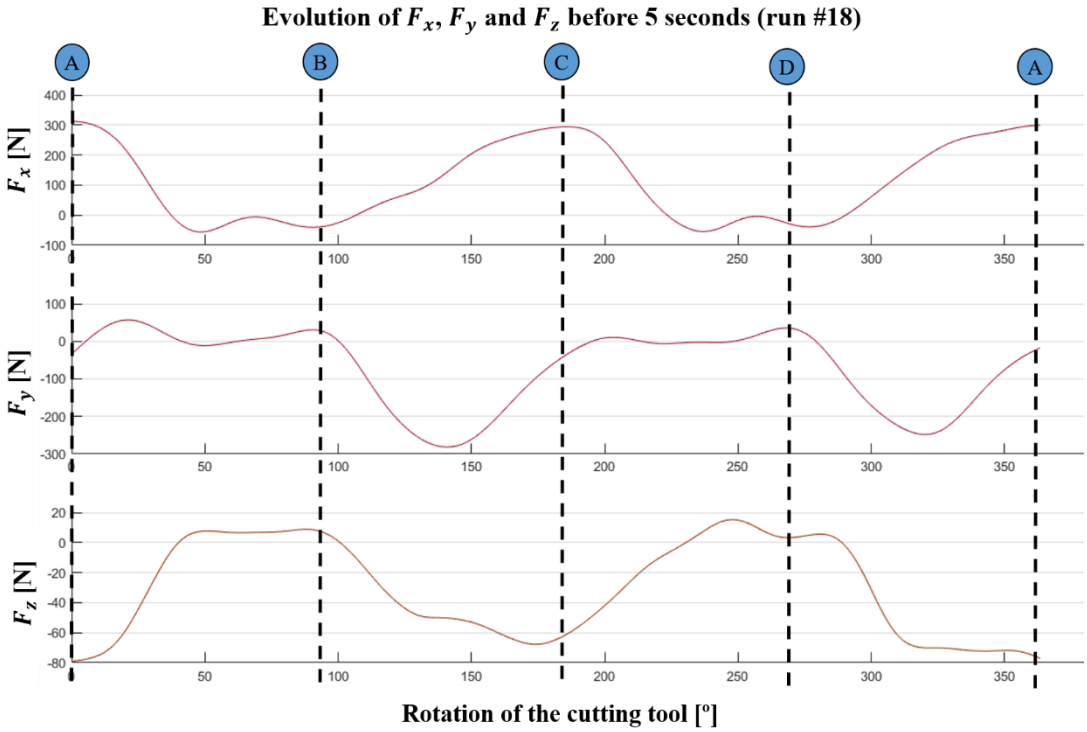

Figure 5.5 Evolution of F_x, F_y and F_z before 5 seconds

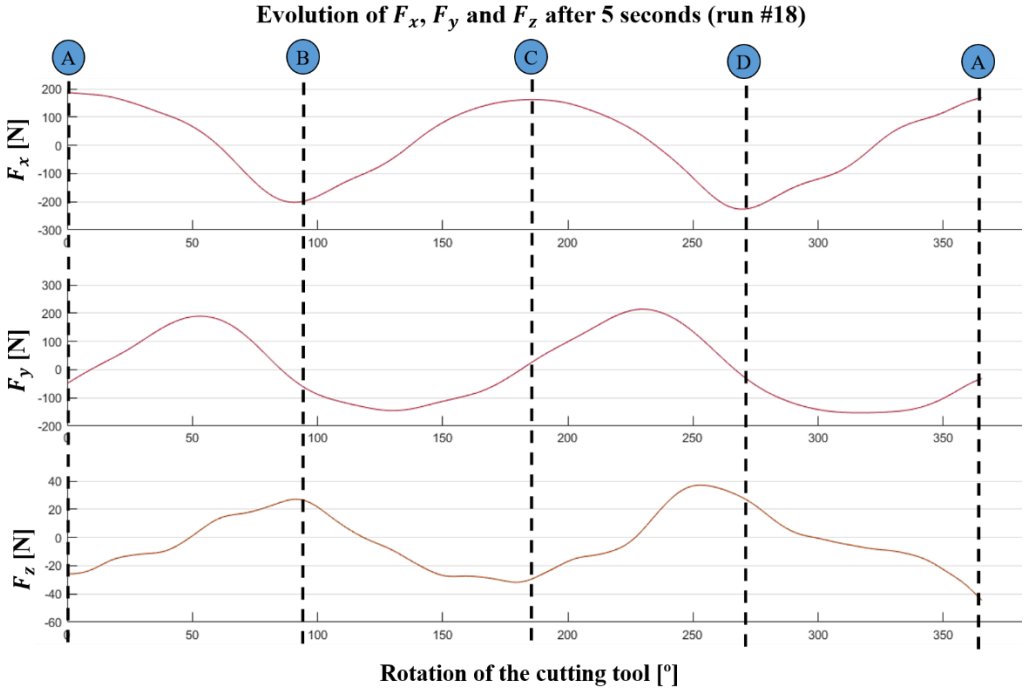

Figure 5.6 Evolution of F_x, F_y and F_z after 5 seconds

The evolution of the cutting forces at an early stage of the cutting process (before 5 seconds) is in accordance with the literature. When the reference cutting edge is in position A, the cutting area is at its maximum level. Thus, F_x (correspondent to the cutting force at this point) reaches its maximum value at this position. At this point, the value of F_y is approximately zero. After the red cutting edge pass by position A, F_x starts to decrease due to the reduction of the cutting area and simultaneously F_y is slightly increased. When the cutting edge leaves the workpiece, which occurs somewhere between positions A and B (around 50º), both F_x and F_y reach approximately 0 N. Then, there is a short period of time (between 50º and 100º) when the cutting forces remain zero, since there is no cutting edge cutting the material.

Thereafter, when the reference cutting edge is somewhere between positions B and C (around 100º), and consequently not cutting the material, the other cutting edge starts to engage the workpiece. Therefore, an increase of F_y can be observed, followed by its reduction as the reference cutting edge approaches position C (it must be noted that the other cutting edge approaches position A), reaching 0 N at this position. Simultaneously, a progressive increase of F_x is noted, until it reaches once again its maximum value when the reference cutting edge is in position C.

Afterwards, between positions C and D, the cutting forces have the same evolution trend as described between positions A and B.

Regarding the evolution of F_z, when the cutting edge starts to engage the workpiece (positions B and D), F_z starts to increase, as the cutting edge enters gradually the cut. This is attributed to the tendency of the cutter to lift the part from the fixture due to the helical geometry of the cutting teeth. As stated before in chapter 2.2.3, for a helical-flute cutter, the cutting edge enters and leaves gradually the cut. The time during which the active portion of the cutting edges remains unaltered (which in this case occurs from approximately 130º to 180º and from approximately 310º to 360º), F_z tends to stabilize. After those instants, the cutter tooth starts to gradually leave the cut, thus causing a decrease in F_z until it reaches approximately 0 N when cutting edge leaves the cut.

Additionally, by observing Figure 5.5, two peaks were registered during one rotational period of the cutting tool. Each peak is related to one cutting edge when reaching the point where the cutting area is maximum. However, it can be noted that the maximum values at each peak are not exactly equal. In this case, the first peak is slightly higher than the second peak. In turn, the second peak is slightly lower than the third one which is equal to the first peak, and so on. This suggests that the peaks vary alternately between two close values, yet distinct. This is due to the offset of the cutting edges. The cutting edges are not exactly identic, revealing the inaccuracy in the radial location of the teeth of the cutting tool, which leads to this small difference between the maximum cutting forces registered.

In contrast, the evolution of the cutting forces observed in Figure 5.6 does not correspond to the typical evolution of the cutting forces during this process. It was already referred that, when the cutting tool is half immersed in the workpiece, at some instants, both cutting edges are cutting the material at the same time. Consequently, this causes the dynamometer to measure charges exerted by two cutting edges simultaneously, thus causing an overlay of the read signal. This contributes to a different evolution of the cutting forces than the one verified previously.

In sum, the analysis above suggests that the maximum cutting forces must be registered during the initial moments of the cutting process, when just one cutting edge is engaged on the workpiece at each moment. At the beginning of the process, for run #18, the maximum cutting

force registered was 307 N, thus contrasting with the 160 N measured when the cutting tool is half immersed in the part, later in the process. This will lead to different specific cutting energy calculations for the same experiment, which indicates that, if the cutting forces acquired during the experiments were not properly analysed, an error could be committed when calculating this indicator.

The maximum cutting forces registered for each experiment and the correspondent specific cutting energy calculations are presented in Appendix A (Table A.1). As expected, it is observed that the maximum cutting force registered occurs for run #08, since it is one of the experiments with the higher cutting area ($f_z = 0.061$ mm/tooth and $p = 4.19$ mm). In contrast, the minimum cutting force verified is related to run #43. This is one of the experiments with the lowest cutting area ($f_z = 0.007$ mm/tooth and $p = 3$ mm). Both values are highlighted in bold.

5.3 Statistical analysis of specific cutting energy

After obtaining the maximum cutting forces for each experiment and, afterwards, the specific cutting energy calculations, the ANOVA technique was employed to reveal the statistical effects of the explored variables on the desired response for a significance level $\alpha = 0.05$, which corresponds to a confidence interval of 95%. This analysis contains the linear, quadratic and interaction terms. Table 5.1 presents the ANOVA table for the specific cutting energy.

The linear term of feed per tooth was the most significant factor for the response variable. This factor has the highest *F-value* of 141.4184, followed by the linear term of depth of cut and the quadratic term of feed per tooth, with *F-value* of 54.4096 and 26.8919, respectively. All the other explored variables, namely the quadratic term of depth of cut, the linear and quadratic terms of cutting speed and the interaction terms between the three cutting parameters, have proved not to be statistically significant for the model, as its *P-value* is higher than 0.05. The percentage contribution was calculated by the quotient between SS of each factor and the total SS. The highest commanding effects on specific cutting energy were attributed to the linear terms of feed per tooth and depth of cut, with contributions of 52.82% and 20.32%, respectively.

Table 5.1 Analysis of variance for specific cutting energy

Factor	SS	Contribution	DOF	MS	*F-value*	*p-value*	Remarks
v_c (L) (1)	0.77884	1.42%	1	0.77884	3.8043	0.058524	
v_c (Q)	0.01273	0.02%	1	0.01273	0.0622	0.804393	
f_z (L) (2)	28.95169	52.82%	1	28.95169	141.4184	< 0.0001	Significant
f_z (Q)	5.50541	10.04%	1	5.50541	26.8919	< 0.0001	Significant
p (L) (3)	11.13892	20.32%	1	11.13892	54.4096	< 0.0001	Significant
p (Q)	0.33244	0.61%	1	0.33244	1.6239	0.210293	
(1) × (2)	0.00004	~ 0%	1	0.00004	0.0002	0.989282	
(1) × (3)	0.00233	~ 0%	1	0.00233	0.0114	0.915625	
(2) × (3)	0.30558	0.56%	1	0.30558	1.4927	0.229330	
Error	7.7795	14.19%	38	0.20472			
Total	55.9443	100%	47				

Therefore, this analysis suggests that both machining parameters feed per tooth and depth of cut deeply affect the specific cutting energy, whereas the effect of cutting speed is not determinant for this indicator. Moreover, the cross effects between the machining parameters are negligible, suggesting that the effect of one parameter is not affected by others.

Next, the RSM was employed to quantify the correlation between the explored variables and the specific cutting energy. The obtained response surface model is given by Equation (5.1).

$$K_s = 3.161978 + 0.137876 \cdot v_c - 0.021405 \cdot {v_c}^2 - 0.840622 \cdot f_z + 0.445074 \cdot {f_z}^2 - 0.521418 \cdot p + 0.109369 \cdot p^2 + 0.001249 \cdot v_c \cdot f_z + 0.009850 \cdot v_c \cdot p + 0.112839 \cdot f_z \cdot p \quad \textbf{(5.1)}$$

For a profound assessment of the model, *R-squared* (R^2) and adjusted *R-squared* (*adj* R^2) were calculated. Statistically, the R^2 represents the proportion of the variance in the output variable that is explained by all the input variables. In this case, the R^2 is equal to 86%, which indicates that 86% of the total variations can be explained by the model. However, if more input variables were added to the experiment, R^2 will increase or stay the same, even if those input variables do not affect the final response of the system. To overcome this question, *adj* R^2 is considered. *Adj* R^2 is a modified version of R^2, that adjust for input variables that have no

significance for the regression model. The regression model revealed and *adj* R^2 of 83%, thereby representing a satisfactory fit for the response variable in study.

The scatter plot of observed values vs predicted values is depicted in Figure 5.7, which suggests that exists an acceptable correlation between the observed values of K_s and the values predicted by the polynomial model. The points are approximately distributed along the red line. Figures 5.8 and 5.9 present the residual analysis of the regression model. The normal probability scatter plot of residuals (Figure 5.8) indicates that the residuals of the model follow a normal distribution. It can be observed that almost all the points in the plot follow the red line. Additionally, the scatter plot of predicted values vs the residual values (Figure 5.9) shows a random distribution of the points, without any significant tendency verified.

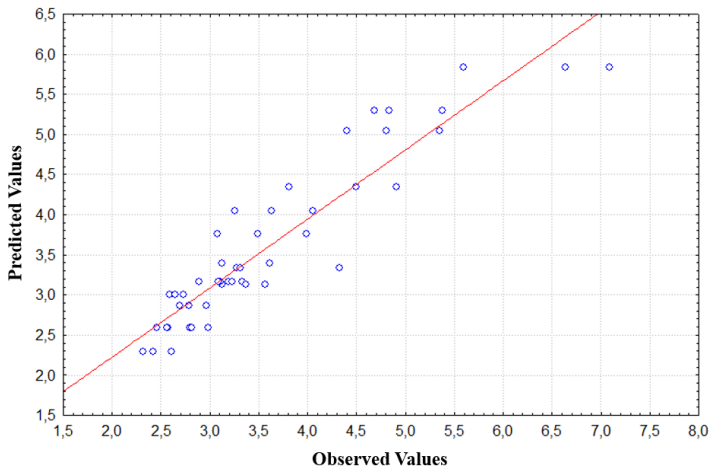

Figure 5.7 Scatter plot of predicted values vs observed values of specific cutting energy

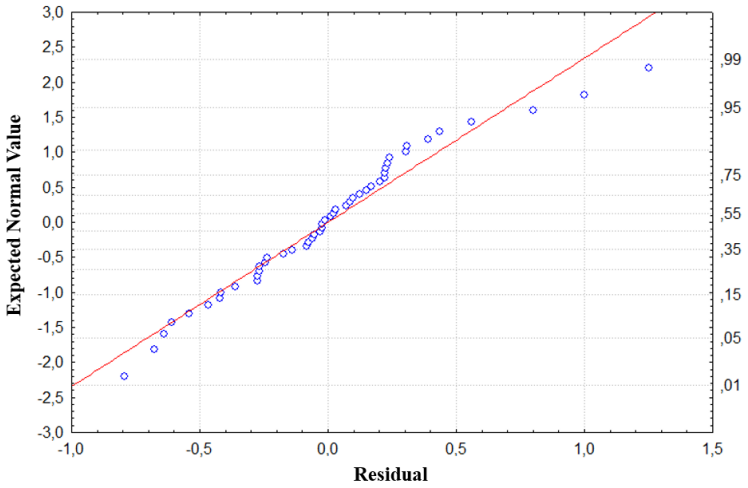

Figure 5.8 Normal probability plot of residuals of specific cutting energy

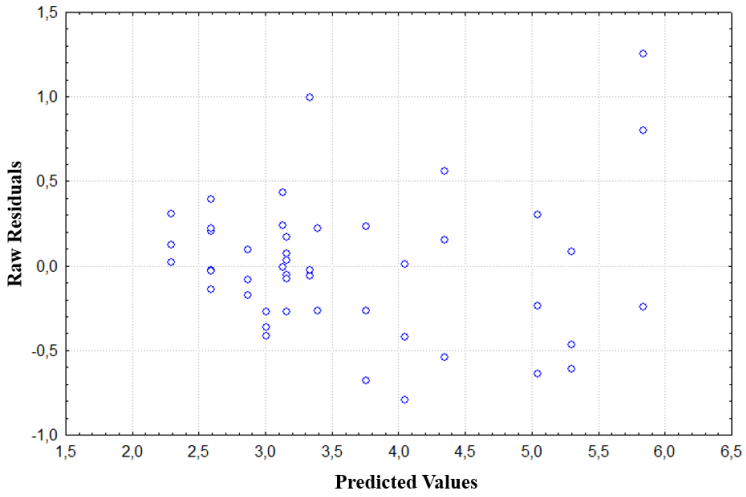

Figure 5.9 Scatter plot of raw residuals vs predicted values of specific cutting energy

The fitted response surfaces and the correspondent fitted response profiles of the regression model are depicted in Figures 5.10 - 5.12. Figure 5.10 exhibits the effects of feed per tooth – depth of cut. It can be observed that an increase in feed per tooth leads to a decrease on specific cutting energy. Moreover, not only the effect of feed per tooth is visible, but also the influence of depth of cut is clearly noted. For the same levels of feed per tooth, an increase in depth of cut leads to the decrease on specific cutting energy.

Figures 5.11 and 5.12 demonstrate the effects feed per tooth – cutting speed and depth of cut – cutting speed. As expected, both figures reveal that, when maintaining feed per tooth and depth of cut constant, the specific cutting energy does not exhibit significant variations when varying the cutting speed, thus highlighting the reduced effect of this factor on specific cutting energy. Once more, the effects of feed per tooth and depth of cut can be seen.

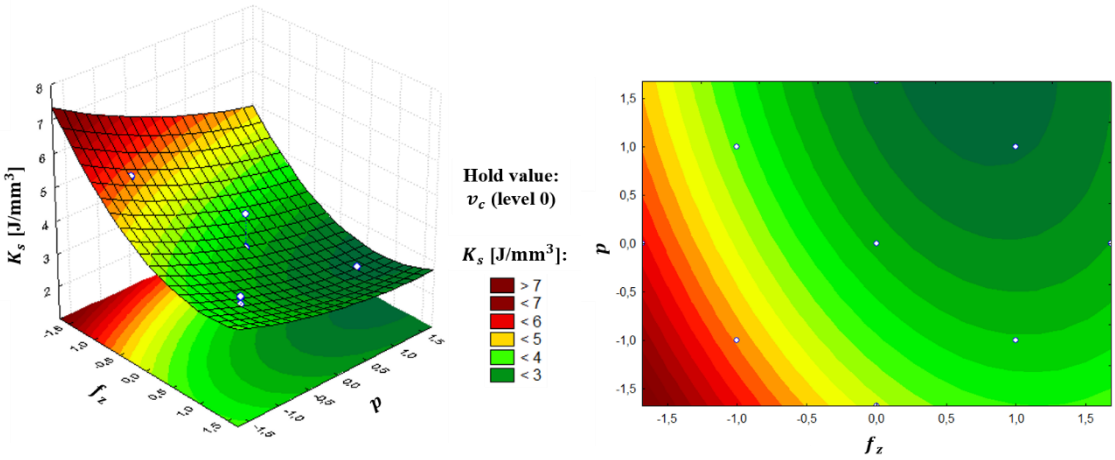

Figure 5.10 Fitted response surface and fitted response profile of specific cutting energy for $f_z \times p$

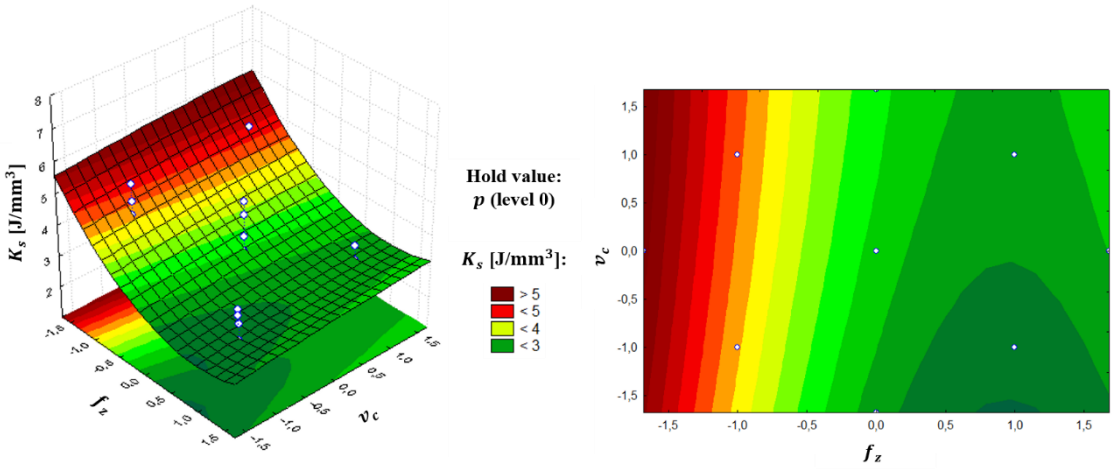

Figure 5.11 Fitted response surface and fitted response profile of specific cutting energy for $f_z \times v_c$

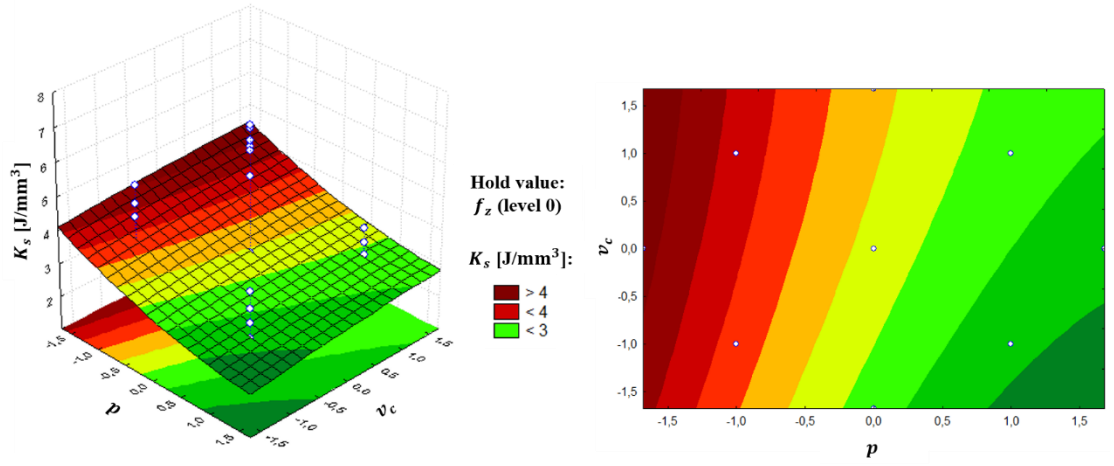

Figure 5.12 Fitted response surface and fitted response profile of specific cutting energy for $p \times v_c$

Once identified the factors whose effect is statistically significant, namely the linear and quadratic terms of feed per tooth and the linear term of depth of cut, a different response surface model was obtained. The non-significant effects of the other factors were ignored. This model, given by Equation (5.2), is similar to the one that considers all factors. The regression coefficients related to the most significant factors (linear terms of feed per tooth and depth of cut) remained unaltered, whereas the remaining coefficients do not change importantly, thus revealing the non-significant effect of the factors disregarded. The estimates of specific cutting energy provided by this model will be further compared to those obtained using the model created for process planning.

$$K_s = 3.259304 - 0.840622 \cdot f_z + 0.419013 \cdot {f_z}^2 - 0.521418 \cdot p \quad \textbf{(5.2)}$$

5.4 Specific Cutting Energy Model for Process Planning

Through RSM, the response surface model as function of feed per tooth and depth of cut was obtained, since these were the cutting parameters whose contributions were statistically significant for the specific cutting energy. However, as stated before, this model must not be used to estimate this quantity. Instead, considering both influent parameters, a new series of experiments was defined with the purpose of formulating a simple and more practical model to estimate the specific cutting energy, similar to those presented in chapter 2.2.5.2 and whose appearance is given by Equation (5.3).

$$K_s = \frac{C}{{f_z}^a \cdot p^b} \quad \textbf{(5.3)}$$

The values of feed per tooth and depth of cut considered for the new series of experiments are listed in Table 5.2. The cutting speed v_c was kept constant at the value recommended by the tool manufacturer. The experiments were conducted according to the experimental plan defined in Table 5.3. This new experimental plan comprised two groups of experiments. The first one consisted of varying feed per tooth, while depth of cut was kept constant at an intermediate value, that was 3 mm. The other group consisted of the reverse, that was varying depth of cut, keeping constant feed per tooth at 0.041 mm/tooth. The experimental plan was replicated twice, for a total of 42 runs.

Table 5.2 Values of the cutting parameters for the new series of experiments

Cutting parameters	**Variation values**						
f_z [mm/tooth]	0.021	0.028	0.034	0.041	0.048	0.054	0.061
p [mm]	1.81	2.20	2.60	3.00	3.40	3.80	4.19

Table 5.3 New experimental plan

Run	**Cutting parameters**		
	f_z **[mm/tooth]**	p **[mm]**	v_c **[m/min]**
Ad #1 / Ad #15 / Ad #29	0.021	3	120
Ad #2 / Ad #16 / Ad #30	0.028	3	120
Ad #3 / Ad #17 / Ad #31	0.034	3	120
Ad #4 / Ad #18 / Ad #32	0.041	3	120
Ad #5 / Ad #19 / Ad #33	0.048	3	120
Ad #6 / Ad #20 / Ad #34	0.054	3	120
Ad #7 / Ad #21 / Ad #35	0.061	3	120
Ad #8 / Ad #22 / Ad #36	0.041	1.81	120
Ad #9 / Ad #23 / Ad #37	0.041	2.20	120
Ad #10 / Ad #24 / Ad #38	0.041	2.60	120
Ad #11 / Ad #25 / Ad #39	0.041	3.00	120
Ad #12 / Ad #26 / Ad #40	0.041	3.40	120
Ad #13 / Ad #27 / Ad #41	0.041	3.80	120
Ad #14 / Ad #28 / Ad #42	0.041	4.19	120

The purpose of varying one parameter while keeping the other one constant is to obtain firstly two independent specific cutting energy expressions, each one dependent on a single cutting parameter, whose appearance is given by Equations (5.4) and (5.5). As proved by the results obtained through ANOVA technique, the factors related to the interaction between the cutting parameters, particularly between feed per tooth and depth of cut, are statistically non-significant. This means that the effect of feed per tooth is not affected by depth of cut, and vice-versa. Due to this fact, one machining parameter can be varied while keeping the other constant.

$$K_s = \frac{C_1}{{f_z}^j} \tag{5.4}$$

$$K_s = \frac{C_2}{p^k} \tag{5.5}$$

In Appendix B (Table B.1), the results obtained from the new series of experiments are shown, namely the maximum cutting forces measured and the correspondent specific cutting energy calculations.

Finally, for the same set of machining parameters, the mean specific cutting energy was computed and afterwards plotted as function of feed per tooth and depth of cut (Figures 5.13 and 5.14). The regression models are given by Equations (5.6) and (5.7). Both models present a good fit. The percentage of the total variations explained by the models (R^2) dependent on feed per tooth and depth of cut are respectively 97% and 99%, strongly revealing the adequacy of the models. As expected, a decreasing trend of specific cutting energy is observed when feed per tooth and depth of cut are increased.

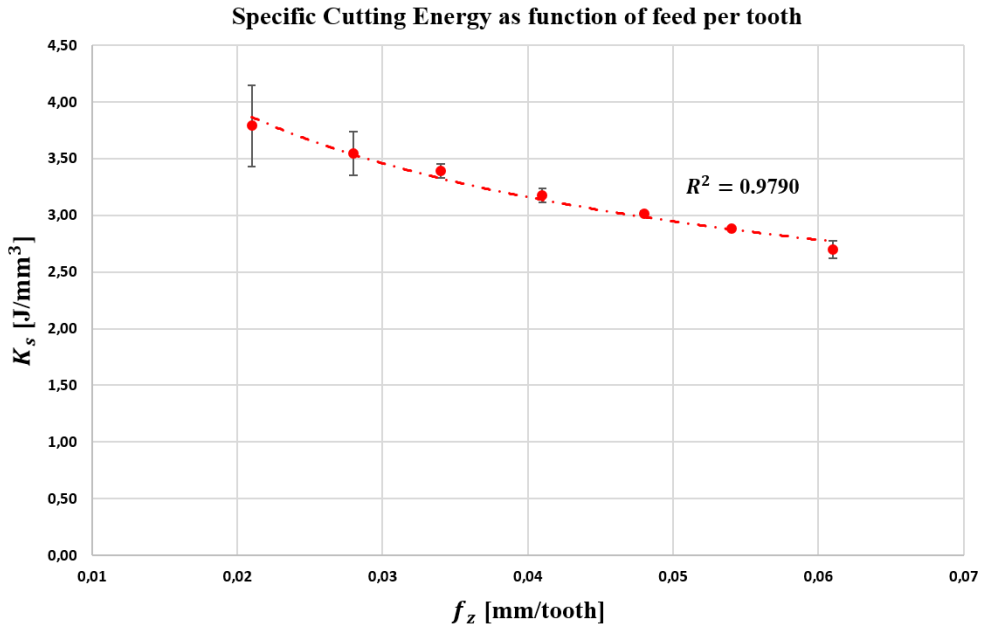

Figure 5.13 Specific cutting energy as function of feed per tooth, for $p = 3$ mm

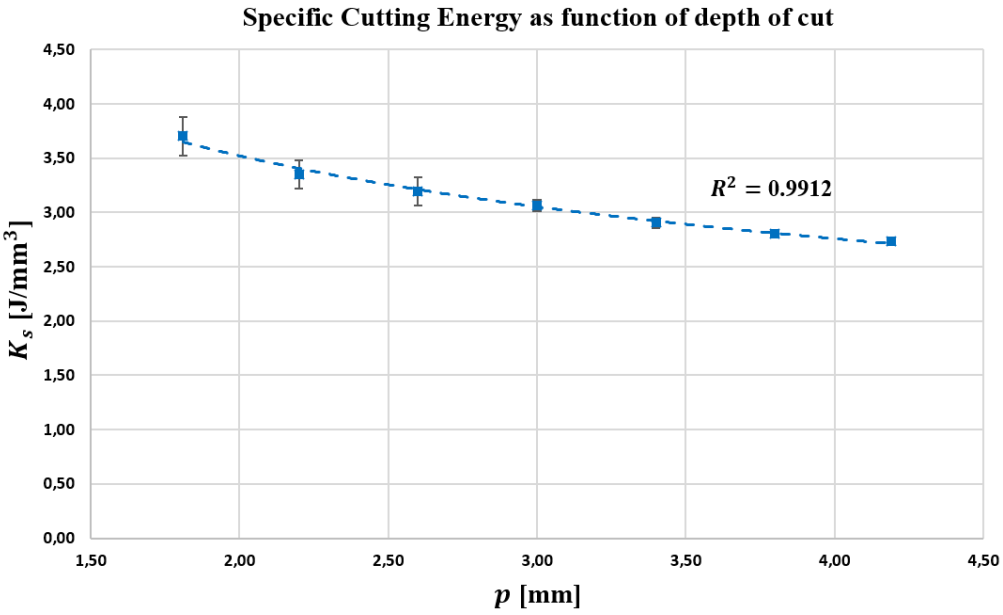

Figure 5.14 Specific cutting energy as function of depth of cut, for f_z = 0.041 mm/tooth

$$K_s = \frac{1.152}{f_z{}^{0.314}} \tag{5.6}$$

$$K_s = \frac{4.496}{p^{0.352}} \tag{5.7}$$

At this stage, the main interest is to combine both Equations (5.6) and (5.7) obtained previously to create a final prediction model. This chapter describes the process inherent to its determination.

Equation (5.6) can be rewritten, in order to obtain a general formula with a similar appearance as the model intended to be formulated, as defined by Equation (5.8). It establishes a correlation between an unknown constant *C* and both machining parameters feed per tooth and depth of cut. The value of *b* is also unknown. Combining both Equations (5.6) and (5.8), another correlation can be obtained. Equation (5.6) is applicable when machining with a depth of cut of 3 mm. Thus, its numerator (1.152) is equal to the quotient between the unknown constant *C* and the term related to the depth of cut, with p = 3 mm. This is explicit in Equation (5.9).

$$K_s = \frac{C}{{f_z}^{0.314} \cdot p^b} \quad \textbf{(5.8)}$$

$$1.152 = \frac{C}{3^b} \quad \textbf{(5.9)}$$

Additionally, Equation (5.10) is obtained replacing p by the numerical value 1 mm on Equation (5.8). Thus, it reflects the specific cutting energy as function of feed per tooth when machining with a depth of cut of 1 mm.

$$K_s = \frac{C}{{f_z}^{0.314}} \quad \textbf{(5.10)}$$

At this point, the main focus is directed towards determination of both values of C and b. Firstly, through Equation (5.7), applicable when machining with a feed per tooth of 0.041 mm/tooth, considering p = 1 mm, it follows that the specific cutting energy equals 4.496 J/mm^3. Afterwards, this result was applied to Equation (5.10), that is valid for a depth of cut of 1 mm. Thus, considering f_z = 0.041 mm/tooth and K_s = 4.496 J/mm^3, the value of C was determined, being equal to 1.649. For last, using Equation (5.9), and replacing C by its numerical value, it was concluded that b = 0.326. The model for the estimation of specific cutting energy, as function of feed per tooth and depth of cut, is given by Equation (5.11).

$$K_s = \frac{1.649}{{f_z}^{0.314} \cdot p^{0.326}} \quad \textbf{(5.13)}$$

Observing the aforementioned expression, it is noted that the impact of feed per tooth on specific cutting energy is slightly lower than the effect of depth of cut ($0.314 < 0.326$). In first instance, this fact goes against the results obtained through ANOVA, in which feed per tooth was identified as the parameter with the major effect on specific cutting energy. However, recovering the model given by Equation (5.2), it can be noted that the effect of the linear term of feed per tooth is counterbalanced by the effect of the quadratic term of this parameter, thus providing more importance to the effect of depth of cut.

5.5 Validation Procedure

After its formulation, the specific cutting energy model was subjected to a validation procedure. For that purpose, several experiments, hereinafter referred to as validation tests, were carried out to ascertain the applicability of the empirical model created.

Once it was proven that the cutting speed was statistically non-significant for the specific cutting energy, this parameter was kept constant at the value recommended by the tool manufacturer. In turn, feed per tooth and depth of cut were randomly varied over the practicable experimental range to which the model applies. Three different combinations of feed per tooth and depth of cut were established and the experiments were replicated twice, for a total of 9 experiments. As before, the cutting forces were measured and the specific cutting energy calculated for each experiment. Table 5.4 shows the validation tests performed. The results are presented in Appendix C (Table C.1).

Table 5.4 Validation tests

Validation test	**Cutting parameters**		
	f_z **[mm/tooth]**	p **[mm]**	v_c **[m/min]**
VT 1 / VT 4 / VT 7	0.031	2.14	120
VT 2 / VT 5 / VT 8	0.043	3.20	120
VT 3 / VT6 / VT 9	0.057	3.97	120

Firstly, the average value between the three replicates of each set of cutting parameters of the validation tests was compared to the estimates provided by the model formulated. Table 5.5 resumes the obtained results, which are plotted in Figure 5.16.

Table 5.5 Comparative analysis between K_s (validation tests) and K_s (model)

Validation tests	K_s **(validation tests) [J/mm^3]**	K_s **(model) [J/mm^3]**	**Error [%]**
VT 1 / VT 4 / VT 7	3.80	3.83	1
VT 2 / VT 5 / VT 8	2.81	3.03	8
VT 3 / VT6 / VT 9	2.47	2.59	5

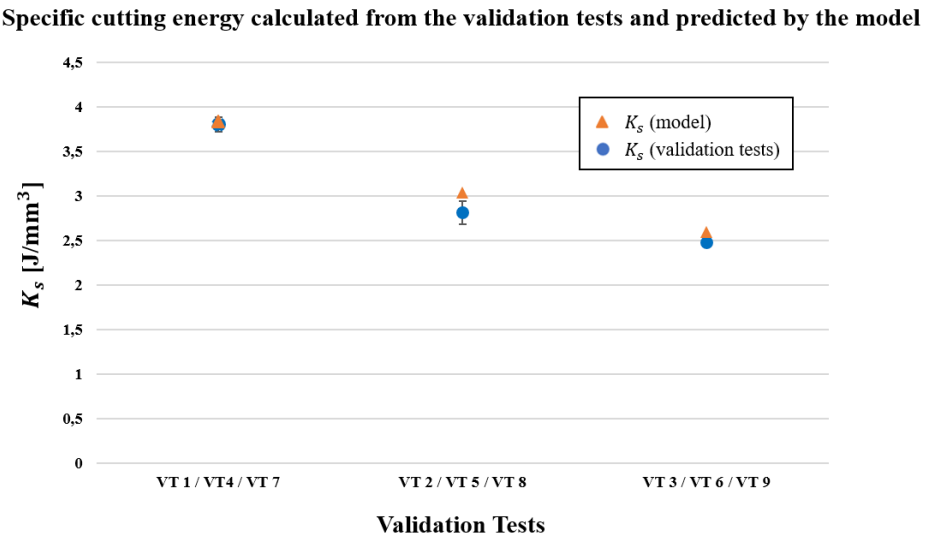

Figure 5.15 Comparative analysis between K_s (model) and K_s (validation tests)

A good agreement between the results of the validation tests and the predicted values by the model is observed. In all cases, the estimates of the model were higher than the values obtained from the validation tests, which means that the forecasts are slightly overestimated, which is appropriate in terms of process planning. The maximum relative error obtained was 8%, relative to experiments VT 2, VT 5 and VT 8. Thereby, the results justify the legitimacy of the model.

Subsequently, once formulated a model of specific cutting energy dependent on the cutting parameters, it is possible to estimate the cutting forces inherent to the process. Thus, although this analysis is redundant, using the specific cutting energy estimates provided by the model, the cutting forces were firstly calculated through Equation (2.14), already presented in chapter 2.2.5.1. Then, the cutting forces estimates were compared to the cutting forces measured during the validation tests. The results are presented in Table 5.6 and plotted in Figure 5.17.

The cutting forces estimated from the specific cutting energy forecasts provided by the model are consistent with the cutting forces measured during the validation tests. Once more, the verified results are always overestimated. As expected, the errors between the experimental results and the forecasts provided by the model are equal to those obtained when comparing the values of specific cutting energy.

Table 5.6 Comparative analysis between F_c (validation tests) and F_c (model)

Validation tests	F_c (validation tests) [N]	F_c (model) [N]	Error [%]
VT 1 / VT 4 / VT 7	252	254	1
VT 2 / VT 5 / VT 8	386	417	8
VT 3 / VT6 / VT 9	558	585	5

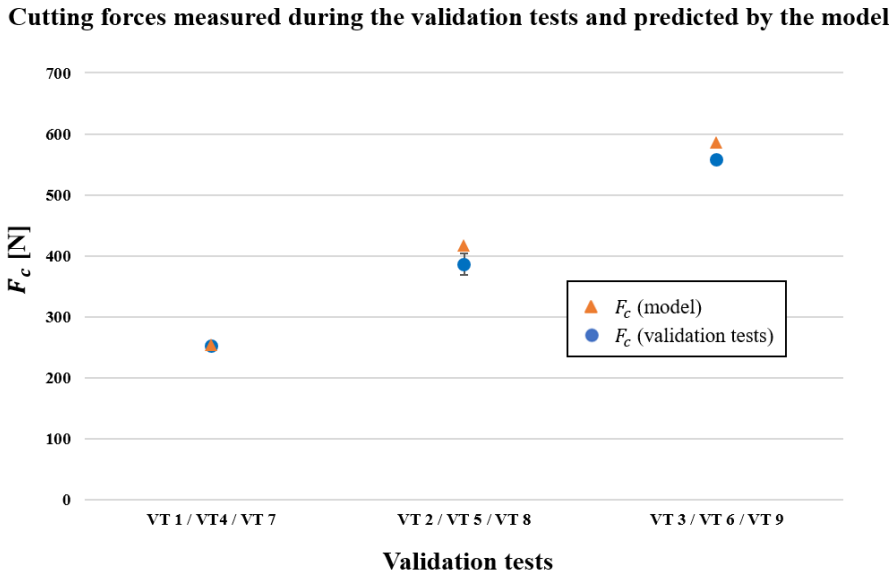

Figure 5.16 Comparative analysis between F_c (model) and F_c (validation tests)

Moreover, an extended analysis was conducted to note the impact of depth of cut on specific cutting energy. As observed in chapter 2.2.5.2, excluding the models proposed by Taylor for cast irons, the effect of depth of cut is not usually considered for the models. Thus, instead of comparing the results from the validation tests with the estimates provided by the model formulated, the results will be compared to those obtained using Equation (5.6), which allows to estimate the specific cutting energy only as function of feed per tooth, thus disregarding the effect of depth of cut. The results are summarized in Table 5.7 and depicted in Figure 5.18.

Table 5.7 Comparative analysis between K_s (validation tests) and K_s (Equation (5.6))

Validation tests	K_s (validation tests) [J/mm^3]	K_s (Equation (5.6)) [J/mm^3]	Error [%]
VT 1 / VT 4 / VT 7	3.80	3.43	-10
VT 2 / VT 5 / VT 8	2.81	3.09	10
VT 3 / VT6 / VT 9	2.47	2.83	15

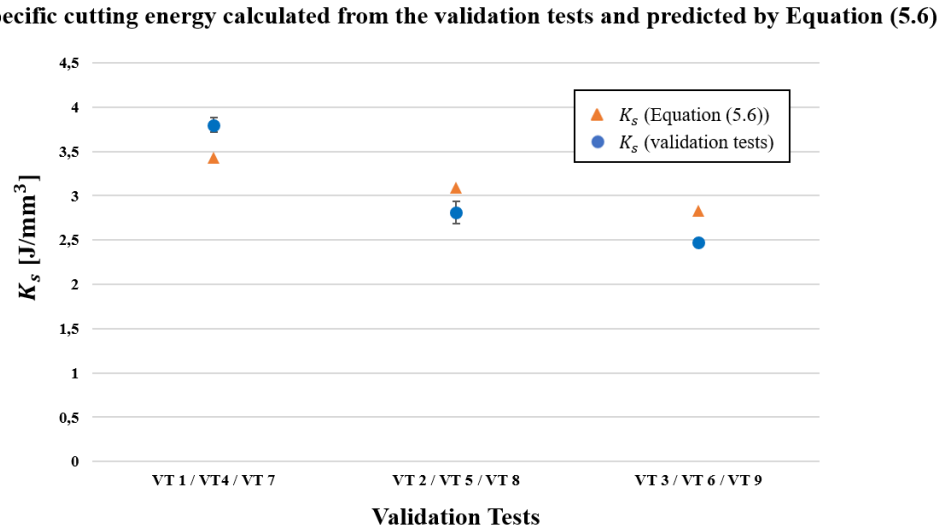

Figure 5.17 Comparative analysis between K_s (Equation (5.6)) and K_s (validation tests)

Firstly, in comparison to the results presented in Table 5.5, the error calculated in respect to the results of the validation tests increased for all the experiments. Moreover, it can be observed from Table 5.7 that, for the experiments with higher values of feed per tooth and depth of cut (VT 3, VT 6 and VT 9), the error is larger (15%) in comparison with the other validation tests (-10% and 10%). This can be attributed to the significance of depth of cut. Thus, it is expected that, for higher values of depth of cut, the non-inclusion of this parameter in the model leads to a larger error.

Additionally, the forecast relative to experiments VT 1, VT 4 and VT 7 was underestimated. From the response surface model, it was observed that lower values of depth of cut lead to an increase of specific cutting energy. Therefore, when disregarding the effect of depth of cut, the specific cutting energy value estimated by Equation (5.6) will be lower than expected because the contribution of that factor for the increase of specific cutting energy is ignored. In terms of process planning this is a problem because lower values of specific cutting

energy are being estimated than those that will actually occur. In contrast, the estimates provided by Equation (5.6) for experiments VT 2, VT 5 and VT 8 and VT 3, VT 6 and VT 9 were overestimated. Likewise, through the response surface model, it was noticed that higher values of depth of cut lead to a decrease of specific cutting energy. Thus, the specific cutting energy values estimated by Equation (5.6) are higher than expected because depth of cut, which contributes for the decrease of this indicator, was not considered.

The results clearly reflect the impact of depth of cut and the importance of including this parameter in the model formulated.

5.6 Comparative Analysis Between the Results of the Validation Tests and the Estimates Provided by Other Models

At this stage, the empirical model has already been validated, which provided good estimates of specific cutting energy. Additionally, a comparative analysis between the results derived from the validation tests and those predicted by other empirical models was performed. To this end, for the same set of cutting parameters used in the validation tests, the specific cutting energy was estimated according to the models provided by ASME, AWF, Taylor and Dormer. The constants used in the models are presented in Appendix D (Table D.1).

Further, the estimates were compared to the results of the validation tests, by calculating the relative error between them. The results are presented in Tables 5.8 - 5.11. Figure 5.19 shows the plotted results.

Table 5.8 Comparative analysis between K_s (validation tests) and K_s (ASME)

Validation tests	K_s (validation tests) [J/mm^3]	K_s (ASME) [J/mm^3]	Error [%]
VT 1 / VT 4 / VT 7	3.80	4.57	20
VT 2 / VT 5 / VT 8	2.81	4.28	52
VT 3 / VT6 / VT 9	2.47	4.04	64

Table 5.9 Comparative analysis between K_s (validation tests) and K_s (AWF)

Validation tests	K_s (validation tests) [J/mm^3]	K_s (AWF) [J/mm^3]	Error [%]
VT 1 / VT 4 / VT 7	3.80	8.39	121
VT 2 / VT 5 / VT 8	2.81	7.18	156
VT 3 / VT6 / VT 9	2.47	6.27	154

Table 5.10 Comparative analysis between K_s (validation tests) and K_s (Taylor)

Validation tests	K_s (validation tests) [J/mm^3]	K_s (Taylor) [J/mm^3]	Error [%]
VT 1 / VT 4 / VT 7	3.80	4.77	25
VT 2 / VT 5 / VT 8	2.81	4.39	56
VT 3 / VT6 / VT 9	2.47	4.09	66

Table 5.11 Comparative analysis between K_s (experimental) and K_s (Dormer)

Validation tests	K_s (validation tests) [J/mm^3]	K_s (Dormer) [J/mm^3]	Error [%]
VT 1 / VT 4 / VT 7	3.80	3.21	-16
VT 2 / VT 5 / VT 8	2.81	3.00	7
VT 3 / VT6 / VT 9	2.47	2.84	15

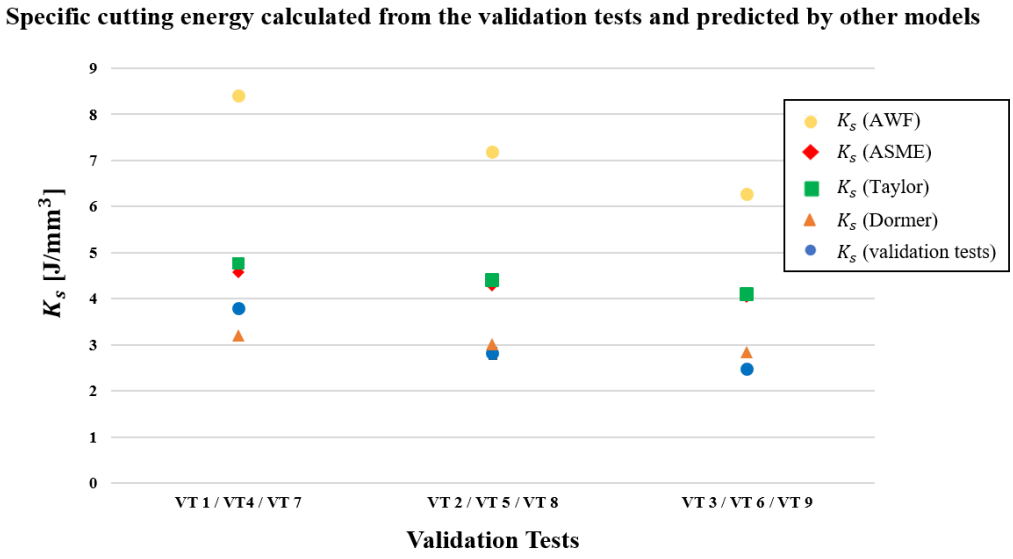

Figure 5.18 Comparative analysis between K_s (other models) and K_s (validation tests)

In first instance, the focus will be directed towards the analysis of the estimates provided by the models proposed by ASME, AWF, and Taylor. It can be noticed that the three models provided less accurate estimates of specific cutting energy than those obtained using the model formulated in the present dissertation. In another words, the error in relation to the results of the validation tests was bigger. The model that provided the least accurate estimates was the AWF model, whose error was higher than 100% for all the validation tests. In turn, the model that led to the closest results from the expected was the model proposed by ASME, whose estimates were similar to those obtained using the model proposed by Taylor.

Moreover, as clearly noted in Figure 5.19, all the specific cutting energy forecasts are overestimated by the models proposed by ASME, AWF and Taylor. As a matter of fact, this was already expected. The empirical models typically used to predict the specific cutting energy are conservative, precisely to enable their widespread use for several types of machining processes, materials and cutting tools. This means that, although the estimates provided by the models may be less precise, they are always higher than the real values. Thus, the feasibility of the operation is ensured due to the conservative character of the models. However, it is not possible to optimise the resources and consequently achieve an efficient process, because the actual values of specific cutting energy are lower than those predicted by these models and from which the process will be planned.

Now, the focus will be directed towards the analysis of the estimates provided by the model proposed by Dormer. The model proposed by this tool manufacturer is not as general as the models proposed by ASME, AWF and Taylor, as it is specified for milling operations and for cutting tools supplied by this manufacturer. Thus, it is expected that the specific cutting energy estimates will be more accurate than those verified before regarding the ASME, AWF and Taylor models, which can be verified by observing the error between the results in Table 5.11.

Additionally, contrary to what was observed previously with the ASME, AWF and Taylor models, the forecasts are not all overestimated. The result regarding the experiments VT 1, VT 4 and VT 7 is underestimated (error of -16%). Moreover, although overestimated, the error concerning the validation tests VT 3, VT 6 and VT 9 is similar (15%). However, it must be noted that these experiments were performed for values of feed per tooth (0.031 mm/tooth and 0.057 mm/tooth, as shown in Table 5.4) different from the value recommended by the tool

manufacturer to machine with the cutting tool and material defined in this dissertation (0.041 mm/tooth, as presented in Table 4.6). Thus, this shows that the model proposed by this tool manufacturer loses its accuracy when machining with cutting parameters values distinct from the recommended values, providing over or underestimated values. Once more, this is attributed to the effect of depth of cut, which was disregarded in this model and that contributes for higher values of specific cutting energy when small values of depth of cut are considered and leads to lower values of this indicator when higher values of depth of cut are applied.

Furthermore, as expected, the experiments whose estimates are closest to the results of the validation tests are VT 2, VT 5 and VT 8 (error of 7%), because were conducted with a value of feed per tooth (0.043 mm/tooth) close to the recommendation.

For last, the experimental results from the validation tests were compared to the response surface model estimates. The results are presented in Table 5.12 and depicted in Figure 5.19.

Table 5.12 Comparative analysis between K_s (validation tests) and K_s (RSM)

Validation tests	K_s (validation tests) [J/mm^3]	K_s (RSM) [J/mm^3]	Error [%]
VT 1 / VT 4 / VT 7	3.80	4.16	9
VT 2 / VT 5 / VT 8	2.81	3.09	10
VT 3 / VT6 / VT 9	2.47	2.43	-2

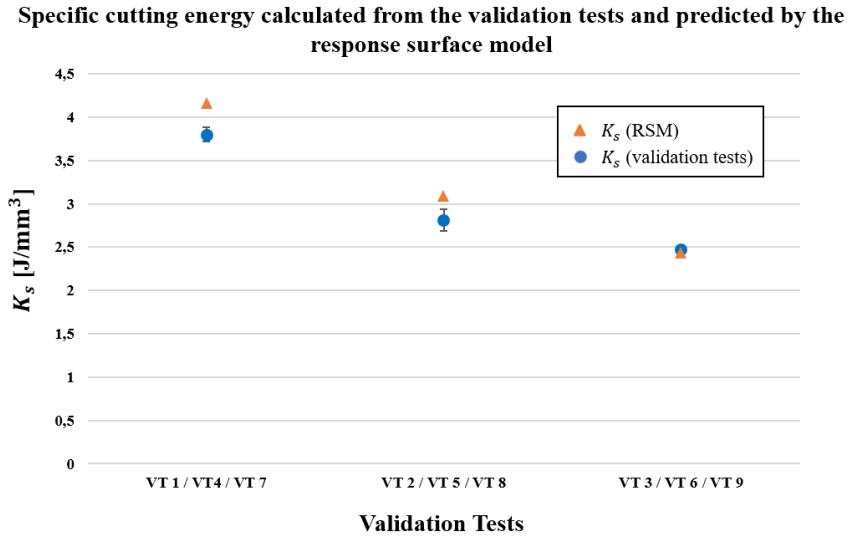

Figure 5.19 Comparative analysis between K_s (MSR) and K_s (validation tests)

As expected, the estimates obtained through the response surface model are close to the results of the validation tests, and consequently to the estimates provided by the model formulated. Regarding the experiments VT 1, VT 4 and VT 7 and VT 2, VT 5 and VT 8, the error is higher in both cases when compared to the estimates provided by the model formulated. Instead, in case of VT 3 / VT 6 / VT 9, the experimental error is lower.

6

CONCLUSIONS AND FUTURE WORK

The main objective of this dissertation was to develop a comprehensive step-by-step methodology for developing specific cutting energy models. In this study in particular, for application in end milling of 1.2738 HH tool steel. This simple and practical model as function of the cutting parameters is a powerful and reliable tool for process planning, as it allows to predict the specific cutting energy accurately and thus achieve an efficient process.

In a first stage, DoE, ANOVA and RSM techniques were applied in order to statistically evaluate the influence of the cutting parameters, namely feed per tooth, cutting speed and depth of cut, on specific cutting energy, for the particular combination cutting operation / workpiece material / cutting tool selected earlier and, for last, to quantify that influence. For this purpose, an experimental plan was developed according to the CCD. After its execution, the cutting forces were successfully measured and specific cutting energy calculated for each experiment. Then, ANOVA technique aided to identify the cutting parameters whose effect was statistically significant for the specific cutting energy and afterwards a response surface model was obtained, which enabled to quantify the correlation between these influent cutting parameters and the specific cutting energy and to gain a better understanding about the response system.

Thereafter, the results obtained through this statistical analysis contributed for the development of an additional experimental plan considering only the statistically significant cutting parameters identified before, which ultimately permitted to establish a simple and practical model to predict the specific cutting energy accurately as function of these cutting parameters.

Finally, the model was subjected to a validation procedure and a comparative analysis between the estimates provided by the model formulated and those obtained by other empirical models was conducted.

Based on the experimental results obtained during this dissertation, the main conclusions were drawn:

- A proper analysis of the cutting force measurements was essential for a better comprehension of the process dynamics, in order to determine which force value must be used to calculate specific cutting energy. Thus, this procedure successfully enabled to achieve an accurate calculation of this indicator.

- ANOVA revealed that feed per tooth and depth of cut were the dominant machining parameters for the specific cutting energy, whereas the effect of cutting speed is negligible. Moreover, the interaction terms between the factors does not present a significant impact on this indicator.

- DoE and RSM techniques proved to be reliable tools for a better understanding of the overall response system. These statistical analyzes allowed to quantify the existing correlation between the cutting parameters (feed per tooth, cutting speed and depth of cut) and the specific cutting energy, through a regression model. From a methodological perspective, it was pertinent to pursue from the results acquired through these methods, in order to obtain a simpler and more practical model to estimate specific cutting energy than the response surface model.

- The model formulated provided accurate estimates of specific cutting energy. The maximum error between the results predicted by the model and those obtained during the validation tests was 8%. Additionally, the forecasts provided by the model were always overestimated, which is appropriate in terms of process planning.

- The models proposed by ASME, AWF and Taylor are conservative, thus enabling its general use for several machining processes, cutting tools and materials. Therefore, as expected, the estimates provided by these models were less accurate than those obtained using the model formulated, and always overestimated. The

model that provided the least accurate forecasts was the AWF model, whose experimental errors were higher than 100%, whereas the model proposed by ASME provided the most accurate results, in which the minimum experimental error verified was equal to 20%.

- As expected, in comparison with the ASME, AWF and Taylor models, the model proposed by Dormer was the most accurate, as it is specified for milling operations and cutting tools supplied by this manufacturer. When machining with cutting parameters values close to the recommendations by this tool manufacturer, the experimental error was equal to 7%. However, the model lost its accuracy when performing experiments considering cutting parameters values different from the recommendations, which is attributed to the effect of depth of cut disregarded for the model.

In sum, it must be stated that the objective proposed for this dissertation was successfully achieved. This study revealed an adequate methodology that led to a simple and practical model to estimate the specific cutting energy accurately, which is a robust and credible tool to achieve an efficient process. This model enables not only to properly select the cutting parameters that lead to a lower specific cutting energy, but also to estimate the cutting forces inherent to the milling process, which in turn are critical to predict the power requirements of the machine tools.

Further investigations related to this subject should be carried out, in order to develop comprehensive methodologies to formulate specific cutting energy models specified for different materials, cutting tools and machining operations, particularly for roughing operations, in which large quantities of material are removed, leading to higher energy consumption. Thus, the correct estimation of specific cutting energy is more relevant for these operations in order to optimise the available resources and achieve an efficient process.

REFERENCES

[1] United States Energy Information Administration, *Anual Energy Review 2011*, 2012 .

[2] G. Y. Zhao, Z. Y. Liu, Y. He, H. J. Cao, and Y. B. Guo, "Energy consumption in machining: Classification, prediction, and reduction strategy," *Energy*, vol. 133, pp. 142–157, 2017, doi: 10.1016/j.energy.2017.05.110.

[3] C. Yuan, Q. Zhai, and D. Dornfeld, "A three dimensional system approach for environmentally sustainable manufacturing," *CIRP Annals - Manufacturing Technology*, vol. 61, no. 1, pp. 39–42, 2012, doi: 10.1016/j.cirp.2012.03.105.

[4] L. Zhou, J. Li, F. Li, Q. Meng, J. Li, and X. Xu, "Energy consumption model and energy efficiency of machine tools: A comprehensive literature review," *Journal of Cleaner Production*, vol. 112, pp. 3721–3734, 2016, doi: 10.1016/j.jclepro.2015.05.093.

[5] E. Müller, R. Poller, H. Hopf, and M. Krones, "Enabling energy management for planning energy-efficient factories," *Procedia CIRP*, vol. 7, pp. 622–627, 2013, doi: 10.1016/j.procir.2013.06.043.

[6] S. T. Newman, A. Nassehi, R. Imani-Asrai, and V. Dhokia, "Energy efficient process planning for CNC machining," *CIRP Journal of Manufacturing Science and Technology*, vol. 5, no. 2, pp. 127–136, 2012, doi: 10.1016/j.cirpj.2012.03.007.

[7] M. Mia, "Multi-response optimization of end milling parameters under through-tool cryogenic cooling condition," *Measurement*, vol. 111, no. July, pp. 134–145, 2017, doi: 10.1016/j.measurement.2017.07.033.

[8] A. P. Markopoulos, W. Habrat, N. I. Galanis, and N. E. Karkalos, "Modelling and Optimization of Machining with the Use of Statistical Methods and Soft Computing," *Design of Experiments in Production Engineering*, no. February, pp. 39–88, 2016, doi: 10.1007/978-3-319-23838-8_2.

[9] C. Camposeco-Negrete, “Optimization of cutting parameters using Response Surface Method for minimizing energy consumption and maximizing cutting quality in turning of AISI 6061 T6 aluminum,” *Journal of Cleaner Production*, vol. 91, pp. 109–117, 2015, doi: 10.1016/j.jclepro.2014.12.017.

[10] G. Campatelli, L. Lorenzini, and A. Scippa, “Optimization of process parameters using a Response Surface Method for minimizing power consumption in the milling of carbon steel,” *Journal of Cleaner Production*, vol. 66, pp. 309–316, 2014, doi: 10.1016/j.jclepro.2013.10.025.

[11] S. H. Imran Jaffery, M. Younas, M. Khan, and L. Ali, “Energy Consumption Analysis in Turning Ti-6Al-4V alloy,” *11th International Conference on Mechanical and Intelligent Manufacturing Technologies*, pp. 18–21, 2020, doi: 10.1109/ICMIMT49010.2020.9041194.

[12] D. O. de Lima, A. C. Araujo, and J. L. L. da Silveira, “Influência da Profundidade de Corte e do Avanço no Frsamento de Facejamento,” *CONEM 2012 - VII Congresso Nacional de Engenharia Mecânica*, pp. 1–9, 2012.

[13] B. Wang, Z. Liu, Q. Song, Y. Wan, and Z. Shi, “Proper selection of cutting parameters and cutting tool angle to lower the specific cutting energy during high speed machining of 7050-T7451 aluminum alloy,” *Journal of Cleaner Production*, vol. 129, pp. 292–304, 2016, doi: 10.1016/j.jclepro.2016.04.071.

[14] M. Mia, “Mathematical modeling and optimization of MQL assisted end milling characteristics based on RSM and Taguchi method,” *Measurement*, vol. 121, pp. 249-260, 2018, doi: 10.1016/j.measurement.2018.02.017.

[15] D. Ferraresi, *Fundamentos da Usinagem dos Metais*, Blucher, 1970.

[16] J. Pamies Teixeira, *Fundamentos Físicos do Corte dos Metais*, EDINOVA, 1999.

[17] “Bem-vindo a Sandvik Coromant,”. [Online]. Available: https://www.sandvik.coromant.com/pt-pt/pages/default.aspx. [Accessed: 02 - September - 2022].

[18] V. Arshinov and G. Alekseev, *Metal Cutting Theory and Cutting Tool Design*, Mir Publishers, 1976.

[19] T. D. Hoang, N. T. Nguyen, Đ. Q. Tran, and N. Van Thien, “Cutting forces and surface roughness in face-milling of SKD61 hard steel,” *Strojniski Vestnik - Journal of Mechanical Engineering*, vol. 65, no. 6, pp. 375–385, 2019, doi: 10.5545/sv-jme.2019.6057.

[20] D. Cica, B. Sredanovic, G. Lakic-Globocki, and D. Kramar, “Modeling of the cutting forces in turning process using various methods of cooling and lubricating: An artificial intelligence approach,” *Advances in Mechanical Engineering*, 2013, doi: 10.1155/2013/798597.

[21] J. L. S. Ribeiro, A. M. Abrão, and W. F. Sales, “Forças de usinagem no fresamento de aços para matrizes,” *Simpósio Pós-graduação em Engenharia Mecânica*, 2015.

[22] A. E. Bayoumi, G. Yücesan, and D. V. Hutton, “On the closed form mechanistic modeling of milling: Specific cutting energy, torque, and power,” *Journal of Materials Engineering and Performance*, vol. 3, no. 1, pp. 151–158, 1994, doi: 10.1007/BF02654511.

[23] V. A. Balogun, H. Gu, and P. T. Mativenga, “Improving the integrity of specific cutting energy coefficients for energy demand modelling,” *Proceedings of the Institution of Mechanical Engineers, Part B: Journal of Engineering Manufacture*, pp. 1–9, 2014, doi: 10.1177/0954405414546145.

[24] A. M. Y. Rigatti, C. L. F. Assis, R. T. Coelho, R. G. Jasinevicius, and A. R. Rodrigues, “Computational method for calculation of the specific cutting energy,” *22nd International Congress of Mechanical Engineering*, pp. 2710-2715, 2013.

[25] “Dormer Pramet,”. [Online]. Available: https://www.dormerpramet.com/ib/es/. [Accessed: 15 - September - 2022].

[26] D. C. Montgomery, *Design and Analysis of Experiments*, 5th edition Wiley, 2001.

[27] D. G. P. G. Hanrahan, J. Zhu, S. Gibani, “Chemometrics and Statistics | Experimental Design, ” *Encyclopedia of Analytical Science*, pp. 8-13, 2005.

[28] J. A. Cornell, *How to Apply Response Surface Methodology*, vol. 8, ASQC, 1990 .

[29] G. E. P. Box and J. S. Hunter, “Multi-Factor Experimental Designs for Exploring Response Surfaces,” *Annals Mathematical Statistics*, vol. 28, no. 1, pp. 195–241, 1957,

doi: 10.1214/aoms/1177707047.

[30] “Statista - The Statistics Portal for Market Data, Market Research and Market Studies,” [Online]. Available: https://www.statista.com/. [Accessed: 07 - September - 2022].

[31] “Haas Automation, Inc. – Ferramentas de Máquina CNC,”. [Online]. Available: https://www.haascnc.com/pt.html. [Accessed: 03 - August - 2022].

[32] “Online Materials Information Resource - MatWab,”. [Online]. Available: https://www.matweb.com/. [Accessed: 22 - September - 2022].

[33] “Sistemas de medição e sensores | Kistler,”. [Online]. Available: https://www.kistler.com/pt/. [Accessed: 03 - August - 2022].

A

RESULTS FROM RSM

Table A.1 Results for $F_{c_{max}}$ and K_s of RSM

Run	Factors (in coded variables)			$F_{c_{max}}$ [N]	K_s [J/mm³]
	v_c	f_z	p		
#1	-1	-1	-1	203	5.35
#2	-1	-1	1	351	3.99
#3	-1	1	-1	394	3.57
#4	-1	1	1	666	2.60
#5	1	-1	-1	205	5.38
#6	1	-1	1	357	4.06
#7	1	1	-1	399	3.61
#8	**1**	**1**	**1**	**715**	**2.80**
#9	-1.68	0	0	365	2.97
#10	1.68	0	0	533	4.33
#11	0	-1.68	0	147	6.63
#12	0	1.68	0	580	2.59
#13	0	0	-1.68	201	4.91
#14	0	0	1.68	612	2.99
#15	0	0	0	393	3.19
#16	0	0	0	410	3.33
#17	-1	-1	-1	183	4.81
#18	-1	-1	1	307	3.49
#19	-1	1	-1	345	3.12
#20	-1	1	1	619	2.42
#21	1	-1	-1	184	4.83

#22	1	-1	1	319	3.63
#23	1	1	-1	345	3.12
#24	1	1	1	658	2.57
#25	-1.68	0	0	343	2.79
#26	1.68	0	0	403	3.27
#27	0	-1.68	0	157	7.09
#28	0	1.68	0	592	2.65
#29	0	0	-1.68	184	4.50
#30	0	0	1.68	577	2.82
#31	0	0	0	383	3.11
#32	0	0	0	398	3.23
#33	-1	-1	-1	167	4.40
#34	-1	-1	1	271	3.08
#35	-1	1	-1	372	3.37
#36	-1	1	1	593	2.32
#37	1	-1	-1	178	4.69
#38	1	-1	1	286	3.25
#39	1	1	-1	399	3.62
#40	1	1	1	628	2.45
#41	-1.68	0	0	331	2.69
#42	1.68	0	0	407	3.31
#43	**0**	**-1.68**	**0**	**124**	**5.59**
#44	0	1.68	0	612	2.73
#45	0	0	-1.68	156	3.81
#46	0	0	1.68	526	2.57
#47	0	0	0	355	2.89
#48	0	0	0	380	3.09

..

B

RESULTS FROM THE NEW EXPERIMENTS

Table B.1 Results for $F_{c_{max}}$ and K_s of the new experiments

Run	Cutting parameters			$F_{c_{max}}$ [N]	K_s [J/mm³]
	f_z [mm/tooth]	p [mm]	v_c [m/min]		
Ad #1	0.021	3	120	219	3.47
Ad #2	0.028	3	120	301	3.58
Ad #3	0.034	3	120	339	3.32
Ad #4	0.041	3	120	383	3.12
Ad #5	0.048	3	120	436	3.03
Ad #6	0.054	3	120	467	2.88
Ad #7	0.061	3	120	490	2.68
Ad #8	0.041	1.81	120	286	3.85
Ad #9	0.041	2.20	120	303	3.36
Ad #10	0.041	2.60	120	325	3.05
Ad #11	0.041	3.00	120	383	3.12
Ad #12	0.041	3.40	120	400	2.87
Ad #13	0.041	3.80	120	440	2.83
Ad #14	0.041	4.19	120	470	2.74
Ad #15	0.021	3	120	234	3.72
Ad #16	0.028	3	120	280	3.34
Ad #17	0.034	3	120	349	3.42
Ad #18	0.041	3	120	390	3.17
Ad #19	0.048	3	120	432	3.00
Ad #20	0.054	3	120	466	2.88
Ad #21	0.061	3	120	481	2.63

Ad #22	0.041	1.81	120	260	3.51
Ad #23	0.041	2.20	120	290	3.22
Ad #24	0.041	2.60	120	346	3.24
Ad #25	0.041	3.00	120	370	3.01
Ad #26	0.041	3.40	120	412	2.96
Ad #27	0.041	3.80	120	436	2.80
Ad #28	0.041	4.19	120	469	2.73
Ad #29	0.021	3	120	263	4.18
Ad #30	0.028	3	120	312	3.72
Ad #31	0.034	3	120	351	3.44
Ad #32	0.041	3	120	398	3.24
Ad #33	0.048	3	120	435	3.02
Ad #34	0.054	3	120	467	2.88
Ad #35	0.061	3	120	508	2.78
Ad #36	0.041	1.81	120	278	3.75
Ad #37	0.041	2.20	120	313	3.47
Ad #38	0.041	2.60	120	351	3.29
Ad #39	0.041	3.00	120	377	3.07
Ad #40	0.041	3.40	120	403	2.89
Ad #41	0.041	3.80	120	435	2.79
Ad #42	0.041	4.19	120	470	2.74

C

RESULTS FROM THE VALIDATION TESTS

Table C.1 Results for $F_{c_{max}}$ and K_s of the validation tests

Validation test	Cutting parameters			$F_{c_{max}}$ [N]	K_s [J/mm^3]
	f_z [mm/tooth]	p [mm]	v_c [m/min]		
VT 1	0.031	2.14	120	254	3.83
VT 2	0.043	3.20	120	406	2.95
VT 3	0.057	3.97	120	553	2.45
VT 4	0.031	2.14	120	246	3.71
VT 5	0.043	3.20	120	382	2.78
VT 6	0.057	3.97	120	564	2.49
VT 7	0.031	2.14	120	256	3.86
VT 8	0.043	3.20	120	371	2.70
VT 9	0.057	3.97	120	558	2.47

D

CONSTANTS OF THE MODELS

Table D.1 Constants of the models proposed by ASME, AWF and Dormer

Empirical Model	Constant	Value
ASME	C_a	228
	n	0.2
AWF	C_w	160
Dormer	K_{c1}	1600 N/mm^2
	z	0.2

2022 EDGAR BELO

A COMPREHENSIVE METHODOLOGY FOR DEVELOPING SPECIFIC CUTTING ENERGY MODELS – APPLICATION IN END MILLING OF 1.2738 HH TOOL STEEL

NOVA SCHOOL OF SCIENCE & TECHNOLOGY